AD-A147 849 EXPOSURE MODELLING OF PARTICLE BEAM LITHOGRAPHY(U) 1/1
ROYAL SIGNALS AND RADAR ESTABLISHMENT MALVERN (ENGLAND)
C BROUGHTON ET AL. AUG 84 RSRE-MEMO-3690 DRIC-BR-93107
UNCLASSIFIED F/G 20/8 NL

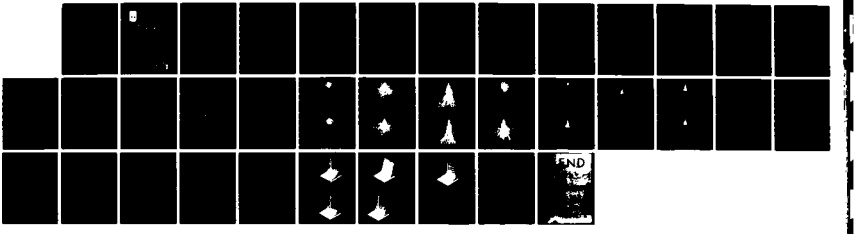

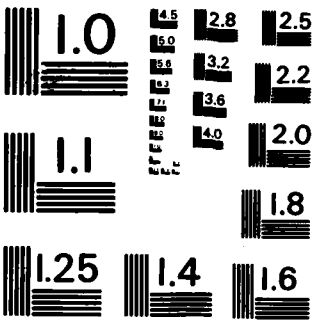

UNLIMITED

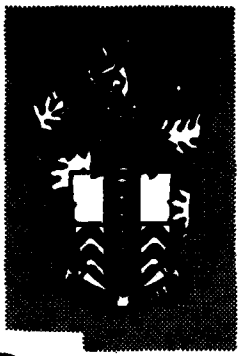

RSRE
MEMORANDUM No. 3690

ROYAL SIGNALS & RADAR ESTABLISHMENT

EXPOSURE MODELLING OF PARTICLE BEAM LITHOGRAPHY

Authors: C Broughton and
V J Mifsud

PROCUREMENT EXECUTIVE,
MINISTRY OF DEFENCE,
RSRE MALVERN,
WORCS.

RSRE MEMORANDUM No. 3690

UNLIMITED

RSRE MEMORANDUM NO 3690

EXPOSURE MODELLING OF PARTICLE BEAM LITHOGRAPHY

C Broughton and V J Mifsud

LIST OF CONTENTS

1 INTRODUCTION

Particle beam lithography depends upon the complex interaction of the incident particle with the polymer resist used. Irradiation of such a polymer by particles causes either polymer chain scission (positive resist) or polymer chain cross-linking (negative resist) giving rise to areas of different solubilities. The change in this property can be used in a differential solubility process using an appropriate organic solvent to remove more soluble areas leaving less soluble areas largely unaffected. This creates a pattern on the substrate that can be used to mask subsequent processing steps.

A detailed understanding of the particle-target interactions is fundamental to being able to produce very small features routinely. In particular it is very important to be able to understand and to compensate for the inevitable proximity effect that is unique to electron beam lithography. This proximity phenomenon can be characterised as two similar, yet distinct, effects:

i. Intra-proximity effect, which is caused by forward scattering of the incident electrons resulting in a reduction of exposure dose (charge/area) and an effective broadening of the incident beam.

ii. Inter-proximity effect, caused by backscattered electrons re-emerging from the substrate and interfering with the exposure of that feature and of neighbouring features.

Ion beam lithography is attractive because the much heavier ions give up their energy very rapidly and undergo very little scattering. Hence, the resist has a greater effective sensitivity to exposure by ions and there are no proximity problems to limit the resolution of the process. However, it is a relatively new technology with which little has yet been achieved and therefore much less information is available about the process and its performance.

To help study and understand the exposure processes of particle beam lithography a computer modelling system has been developed. It was decided to develop a new suite of programmes in order to provide a basis for the investigation of the assumptions and approximations made in the various models and to enable the rapid modification of the system to tackle different cases as these arise in the complementary experimental programme. At the heart of the system is a Monte Carlo simulation programme. This uses random numbers to return values for the scattering angles and step length between interactions with the target nuclei in order to simulate the particle trajectories. The programme stores the energy lost by those particles as they travel through the resist layer to build up an exposure profile for the process.

The study of electron scattering within a material target using a Monte Carlo technique has been investigated in detail by Bishop[1], using the screened Rutherford interaction cross section, Bethe's continuous-slowing-down approximation and Lewis' multiple scattering theory to calculate X-ray production by an electron probe. Adopting the same approach, Shimizu and Murata[2] reported studies on the resolving power and contrast of an SEM concentrating on the backscattered electrons. A change to using the more powerful single scattering model was made by Murata et al[3] and followed by Kyser and Murata[4] in their study of microprobe analysis of thin films on substrates. The first application of this technique to electron beam lithography was made by Shimizu et al[5] and Kyser and Murata[6] which included studies of energy deposition into the resist layer.

Further to these studies Adesida et al[7] have reported results using an extension of Gryzinski's excitation function as a replacement for Bethe's continuous-slowing-down approximation in an attempt to simulate the exposure mechanisms more directly. Also the effect of secondary electrons within the exposure process has been investigated by Murata et al[8], but these are beyond the scope of the work presented here.

and the tactical considerations of the scenario, and to allow for feasible implimentation on a microcomputer, the war game is structured as one replication of a Monte Carlo simulation.

9

Computer studies of ion scattering within solid targets have been reported by many authors. Included amongst these are several dedicated Monte Carlo programmes such as MARLOWE by Robinson and Torrens[9], TRIM by Biersack and Haggmark[10] and PIBER by Adesida and Karapiperis[11&12]. MARLOWE was initially developed to study atomic-displacement cascades with a binary-collision approximation, assuming nuclear scattering governed by the Moliere potential. TRIM also uses Moliere's potential but incorporates a more efficient analytical method for determining scattering angles to study ion transport in amorphous targets. PIBER was developed to study ion exposure of resists for lithographic purposes and uses the experimentally derived universal scattering cross-section of Kalbitzer and Oetzmann[13] and like the previous two uses the electronic stopping formulae of Lindhard et al[14] and Bethe.

In the programmes presented here the scattering model of Kyser and Murata[4&6] is used, with alterations, to simulate the scattering of electrons and Bethe's continuous-slowing-down approximation is assumed to supply a rate of loss of energy by the electrons. A method using Kalbitzer and Oetzmann's universal scattering function, akin to that of Adesida and Karapiperis[11&12], is employed for the ion case and electronic stopping is assumed by Bethe's formulae for high energy ions and by the LSS[14] theory in the low energy regime.

The programmes have been designed to be flexible to allow the user to define an incident beam voltage incident upon an amorphous resist structure, of up to three layers, on top of an amorphous substrate of semi-infinite thickness. They were developed to study exposure processes rather than to be a detailed examination of particle scattering. It is intended that the simulation programmes described within will be expanded to cover the whole lithographic process providing a comprehensive simulation package.

2 THEORY

The scattering model of Kyser and Murata[4&6] is used in the computer simulation of electron beam exposure. For the ion beam case the approach of Anderson and Ziegler[16] is followed, ie the theory of Lindhard et al[13] is assumed for low ion energy levels and at high energy levels the Bohr-Bethe equation is applied, using the interpolation scheme of Verelas and Biersack for the intermediate energy range.

2.1 ELECTRON SCATTERING MODEL

It is assumed that electrons suffer Rutherford scattering within a binary collision process with a target atomic nuclei. The Rutherford differential scattering cross section can be expressed as

$$\frac{d\sigma_i'(\theta)}{d\Omega} = \frac{Z_i(Z_i+1)e^4}{(4\pi\varepsilon_o)^2\, 4E^2(1-\cos\theta+2\alpha_i^2)^2} \qquad (1)$$

where Z_i is the atomic number of the scattering nucleus, e is the electron charge, ε_o is the permittivity of free space, E is the energy of the electron, θ is the scattering angle and α_i is the screening parameter. Strictly equation (1) is not Rutherford's original differential scattering cross section, the $Z_i(Z_i+1)$ factor replaces the usual Z_i^2 factor in the

numerator to allow for inelastic electron-electron scattering and a screening parameter, α_i, is introduced to account for the electronic screening of the target nucleus by its orbital electrons. α_i is given by Cosslet and Thomas[19] as

$$\alpha_i = \frac{\lambda_e Z_i^{1/3}}{4\pi a_o} \qquad (2)$$

where λ_e is the wavelength of the electron and a_o is the Bohr radius of the Hydrogen atom.

The total scattering cross section, σ_i, is achieved by integrating equation (1) between the limits $\theta = 0$ to $\theta = \pi$, ie

$$\sigma_i = \frac{\pi Z_i (Z_i+1)\, e^4}{(4\pi\varepsilon_o)^2\, 4E^2\, \alpha_i^2 (1+\alpha_i^2)} \quad . \qquad (3)$$

2.2 ENERGY LOSS BY ELECTRONS

Bethe's continuous slowing down approximation is assumed to provide a rate of loss of energy by the incident electron as it travels through the target material. The equation for this is

$$\frac{dE}{dS} = -\frac{2\pi e^4 \rho N_a}{(4\pi\varepsilon_o)^2 E} \sum_i \left[\frac{C_i Z_i}{A_i} \ln\left(\frac{\gamma E}{J_i}\right) \right] \qquad (4)$$

where $\gamma = 1.166$, N_a is Avogadro's number, ρ is the density of the target material, C_i is the weight fraction of the i^{th} constituent atomic species and A_i is its atomic mass. J_i is the mean ionisation energy of the nuclei. The values for J_i are given, for $J_i < 13$, by

$$J_i = Z_i (12 + 7\, Z^{-1}) \quad . \qquad (5a)$$

Otherwise by

$$J_i = Z_i (9.76 + 58.5\, Z_i^{-1.19}) \quad . \qquad (5b)$$

2.3 ION SCATTERING MODEL

Ions lose their energy by two major processes due, on the one hand, to elastic Coulomb interactions between the nuclear charges of the ion and target nucleus and, on the other, to inelastic interactions of the incident ion with the electrons within the target. At low energies nuclear stopping dominates the interaction and is responsible for most of the angular dispersion of the incident ions. At higher energies electronic collisions are more important. The theory behind these processes is much less well formulated than in the electron case, especially within the intermediate energy range in which we are working.

2.4 ELECTRONIC STOPPING

In the high energy regime but at non-relativistic ion velocities, the electronic stopping power of the ion is adequately described by the Bohr-Bethe equation

$$\left(\frac{dE}{dS}\right)_B = -\frac{4\pi Z_1^2 C^4 N B}{(4\pi\varepsilon_o)^2 M_e V^2} \tag{6}$$

where Z_1 is the atomic number of the incident ion, N is the number density of target nuclei, M_e is the mass of an electron and B is Bethe's stopping number:

$$B = Z_2 \ln\left(\frac{2M_e V^2}{I}\right) . \tag{7}$$

Here I is the average excitation energy of the target electrons and is given in equations (5a) and (5b). Z_2 is the atomic number of the scattering nuclei.

In the low energy regime, for velocities up to $Z_1^{2/3}\ e^2/\hbar$ the LSS theory can be applied to obtain a rate of loss of energy by the incident ions

$$\left(\frac{dE}{dS}\right)_L = -\xi_e\ 8\pi e^2 N a_o Z_1 Z_2 V/(Z_1^{2/3} + Z_2^{2/3})^{3/2}\ V_o \tag{8}$$

where V_o is the Bohr velocity and ξ_e is a dimensionless constant of the order of $Z_1^{1/6}$.

It is convenient to define a reduced energy

$$\varepsilon = EaM_2(4\pi\varepsilon_o)/(Z_1 Z_2 e^2 (M_1 + M_2)) \tag{9}$$

in which M_1 and M_2 are the respective masses of the incident ion and target nucleus and a is a Thomas-Fermi constant given by

$$a = 0.885\ a_o\ (Z_1^{2/3} + Z_2^{2/3})^{-\frac{1}{2}} \tag{10}$$

and a reduced range

$$\rho_r = RNM_2 a^2 4\pi M_1/(M_1 + M_2)^2 \tag{11}$$

where R is the real range. Using these parameters the LSS theory expresses a rate of loss of energy due to electronic stopping as

$$\left(\frac{d\varepsilon}{d\rho_r}\right)_L = -k\varepsilon^{\frac{1}{2}} \tag{12}$$

where

$$k = \xi_e \frac{0.0793\ Z_1^{\frac{1}{2}} Z_2^{\frac{1}{2}}\ (M_1 + M_2)^{3/2}}{(Z_1^{2/3} + Z_2^{2/3})^{3/4}\ M_1^{3/2}\ M_2^{\frac{1}{2}}} \tag{13}$$

Following Anderson and Zeigler[16], the interpolation scheme of Verelas and Biersack

$$\frac{dE}{dS} = \left[\left(\frac{dE}{dS}\right)_B^{-1} + \left(\frac{dE}{dS}\right)_L^{-1}\right]^{-1} \tag{14}$$

is used to bridge the gap between the high and low energy regimes.

2.5 NUCLEAR STOPPING AND SCATTERING CROSS SECTION

The LSS theory assumes the Thomas-Fermi inter-atomic potential to provide a differential nuclear scattering cross section which can be expressed as

$$d\sigma'(t) = 2\pi a^2 t^{-3/2}\ f(t^{\frac{1}{2}})\ dt \tag{15}$$

where

$$t^{\frac{1}{2}} = \varepsilon \sin\left(\frac{\theta}{2}\right) \tag{16}$$

and ε is the reduced energy of equation (9). The universal scattering function, $f(t^{\frac{1}{2}})$, can be approximated to

$$f(t^{\frac{1}{2}}) = \ell\ t^{\frac{1}{2}-m}\ [1 + (2\ell\ t^{1-m})^q]^{-1/q} \quad . \tag{17}$$

The values of the constants ℓ, m, q, are given by Kalibitzier and Oetzmann[13] as

$$\ell = 2.54 \qquad m = 0.25 \qquad q = 0.475 \quad .$$

The total scattering cross section is assumed to be equal to N (after Adesida and Karapiperis[11]), ie

$$\sigma = \int_{t_{min}}^{t_{max}} d\sigma'(t) = N^{-2/3} \tag{18}$$

where

$$t_{max}^{\frac{1}{2}} = \varepsilon \tag{19a}$$

$$t_{min}^{\frac{1}{2}} = \varepsilon \sin\left(\frac{\theta_{min}}{2}\right) \tag{19b}$$

The nuclear energy loss, ΔE_n, is simply the energy transferred from the incident ion to the target nucleus on collision

$$\Delta E_n = 4M_1M_2(M_1+M_2)^{-2} E \sin^2\left(\frac{\theta}{2}\right) \quad (20)$$

where θ is the scattering angle in the centre of mass system.

3 IMPLEMENTATION

3.1 THE MONTE CARLO METHOD FOR CALCULATING THE PARTICLE SCATTERING PARAMETERS

The probability, $P(\theta)\, d\Omega$, of an incident particle scattering into the solid angle $d\Omega = \sin(\theta)\, d\theta d\Omega$ is given by

$$P(\theta)d\Omega = (\sigma'(\theta)/\sigma)\, d\Omega \quad (21)$$

where σ is the total scattering cross section and $\sigma'(\theta)$ is the fractional scattering cross section, hence, for the electron case

$$\theta = \cos^{-1}\left(1 - \frac{2\alpha_i^2 R_1}{1+\alpha_i^2 - R_1}\right) \quad (22)$$

where R_1 is a uniformly distributed random number between 0 and 1. The ion beam case is less straightforward to implement. The integral of equation (15) cannot be directly evaluated and therefore has to be calculated numerically. A look-up table of I(t) versus t is generated from the integral

$$I(t) = \frac{\pi a^2}{2} \int_t^{t_{ref}} t^{-3/2} f(t^{\frac{1}{2}})\, dt \quad (23)$$

at the start of the computer programme which can then be searched to locate a value for t from which the scattering angle, θ, can be deduced:

$$\theta = 2 \sin^{-1}\left(\frac{t}{\varepsilon^2}\right)^{\frac{1}{2}} \quad . \quad (24)$$

The azimuthal angle is simply given by

$$\phi = 2\pi R_2 \quad (25)$$

where R_2 is a uniformly distributed random number between 0 and 1.

The step length between collisions, S_i, is calculated using Poisson statistics which gives

$$S_i = -\lambda \ln(R_3) \quad . \quad (26)$$

Again R_3 is a uniformly distributed random number between 0 and 1 and λ is the mean free path of the particle. For a mixed element target of i elements, each with weight fraction C_i and atomic mass A_i

$$\lambda = \left[N_a \rho \sum_i \frac{C_i \sigma_i}{A_i} \right]^{-1} \qquad (27)$$

where ρ is the mass density of the target. The probability, P_i, that the incident particle will be scattered by atom i is simply its fraction of the sum of the cross sections, ie

$$P_i = \frac{C_i \sigma_i}{A_i} \Big/ \left(\sum_i \frac{C_i \sigma_i}{A_i} \right) \qquad (28)$$

and can be decided upon by generating a random number, R_4. Hence, if R_4 is in the range $(0 - P_i)$ the particle is assumed to be scattered by an atom of species i, otherwise if R is in the range $(P_i - 1)$ scattering is assumed by a different species. The actual species is determined by comparing R_4 with the ranges 0 to P_1, P_1 to (P_1+P_2) etc. In this manner the scattering species is decided upon in a random yet weighted fashion.

3.2 SEQUENCE OF CALCULATIONS

A particle of energy E_o is incident at 90 deg to the surface of a semi-infinite target. The x-y plane being defined as that of the surface with the particle approaching along the z axis travelling in a +ve z direction (see Figure 1). The step length S_o is calculated by the Monte Carlo method described above, providing the penetration depth before the first scattering event at point 1. The energy lost ΔE_o is deducted from E_o to give a new energy E_1. The scattering angles θ_1, ϕ_1 and step length S_1 are then calculated to arrive at point 2. Again the energy lost is deducted from E_1. This process is repeated until the energy of the incident particle diminishes to an insignificant level, or in the case of electrons, that their projected range is too short and they will not, therefore, re-emerge into the resist film.

The computer programme stores the energy deposited into the resist layer in a 50 by 50 array which corresponds to an imaginary grid of parallelepipeds within the resist film (see Figure 2). The cross sectional area of each parallelepiped is dependent upon the overall dimensions of the simulation but is typically 100 Angstroms square for electrons and 10 Angstroms square for ions. The programme calculates which parallelepipeds the particle passes through between collisions and its path length within the respective elements to deduce the amount of energy deposited into each. This energy is then added to the running total stored in the corresponding array element.

3.3 CONVOLUTION OF THE ENERGY DEPOSITION PROFILE

The computer programme described above assumes that all the particles are incident at the same point on the surface of the resist. Obviously, it is impossible to produce a system with such a beam shape, hence, the energy deposition profile is convoluted with the Gaussian beam profile of a real system to simulate an energy deposition profile for a single pass exposure.

Let E(y,z) be the energy dissipation per unit volume at a lateral distance y and depth z from the origin for the point source and the current distribution of the Gaussian beam be described by

$$C(y) = \exp\left[-0.822\left(\frac{y}{r_o}\right)^2\right] \tag{29}$$

where r_o is the radius of the beam. The beam diameter is defined by the 10%-90% of beam current width. Then the energy distribution for the Gaussian beam system is given by

$$E_g(y,z) = \int_{-\infty}^{\infty} C(r) \cdot E(y-r,z)\, dr \tag{30}$$

4 RESULTS AND DISCUSSION

4.1 TRAJECTORY PLOTS

The figures 3 to 8 show the simulated trajectories for a point source of electrons with incident energies of 10, 20 and 50 keV in two different thicknesses of PMMA resist upon a silicon substrate. They clearly show that the resolution of the electron beam is severely limited by the scattering of the electrons and exhibit the characteristic "pear" shape of the scattering. The broadening of the beam as it travels through the material is caused by forward scattering of the electrons and is known as the intra-proximity effect. It is noticed that this effect can be greatly reduced within the resist layer by increasing the incident beam energy. However, it is also clear that with an increase in beam energy there comes an increase in electron range and consequently an increase in the area affected by the back-scattered electrons. These backscattered electrons can interfere with neighbouring exposures causing the inter-proximity effect. These figures also demonstrate the fact that resolution can be improved through using a thinner resist layer, especially at the lower beam energies, because the resist-substrate interface is brought up higher into the neck of the scattering "pear" where the intra-proximity is less. This, then, can be a very useful method for improving the resolution of electron beam machines of limited beam voltage.

The flexibility of the computer programme is exhibited by figures 9 and 10. Figure 9 shows the simulated trajectories of 100 20 keV electrons incident on to 0.5 microns of PMMA on a Gallium-Arsenide substrate. The problem of increased scatter due to Gallium-Arsenide having a greater density than Silicon is evident. PMMA resist is used here but the programme is capable of simulating any user defined film on any substrate. Figure 10 shows the simulated trajectories of 100 20 keV electrons incident on to a tri-level resist structure consisting of 0.5 microns of PMMA on 0.1 microns of Aluminium on 1.0 microns of PMMA on a silicon substrate. It is noticed that there is marginally less backscatter than in the equivalent one layer case (Figure 6) due to most of the scattering occurring further away from the top of the resist layer.

Figures 11 to 15 show the ion trajectories simulated with 100 keV Gallium into 0.5 microns of PMMA on Silicon, 200 keV Silicon into 0.5 microns of PMMA on Silicon, 200 keV Silicon into 0.2 microns of PMMA on Silicon, 150 keV Silicon into 0.5 microns of PMMA on Silicon, 100 keV Silicon into 0.5 microns of PMMA on silicon respectively. These two species have been simulated as they are available from the liquid metal sources to be supplied with the RSRE/VG 100 kV ion beam lithography machine (IBL100). Comparing these figures with those for the electron beam case the potential for greater resolution is obvious. However, their extremely short range may cause some processing problems. (This will be covered further in a memorandum yet to be published on focussed ion beam systems by V Mifsud.)

4.2 ENERGY DEPOSITION PROFILES

The energy deposition results from the Monte Carlo simulations of electron beams have been convoluted with a Gaussian beam current distribution with a 10% to 90% width of 0.2 microns to provide the equi-energy density contours of Figures 16 to 18. These contours are calculated by joining together those parallelepipeds that contain the same, or nearest, energy value. Each has been formed from the data gathered from simulating 20,000 incident electrons at the same three beam voltages as those of Figures 3 to 8 (10, 20 and 50 keV), into three different thicknesses of PMMA resist, 0.2, 0.5 and 1.0 microns. For example, Figure 16 shows four equi-energy contours for a beam of 10 keV electrons when incident upon 1.0, 0.5 and 0.2 microns of PMMA respectively. These contours are drawn at 20%, 40%, 60% and 80% of the maximum value. Figures 17 and 18 show the same for 20 and 50 keV beam energies. The contour energy values are chosen quite arbitrarily and it is intended that the contours should show the overall energy deposition profile and no attempt is made here to relate these to a developed feature profile although these contours must be important factors in the shaping of the final feature profiles. The effect of using a thinner resist level is more evident from these diagrams, there is a noticeable improvement in resolution, ie less broadening of the profile towards the interface of the resist and substrate, in the 0.2 micron resist layer over the 0.5 and 1.0 micron layers in both the 10 keV and 20 keV case (Figures 16 and 17) but is much less marked in the higher 50 keV case (Figure 18).

Figure 19 shows a comparison of equi-energy levels within a 0.5 micron layer of PMMA after being exposed by 20,000 electrons at the three different energies, 10, 20 and 50 keV. Again the contour energy values are arbitrary and consistent through the three diagrams yet it is clear that the diagrams do not contain the same number of contours. The 10 keV diagram has 5 contours, the 20 keV diagram has 4 having lost the centre contour and the 50 keV diagram has 3 having lost the inner most two. This is because the rate of loss of energy by an electron is inversely proportional to its energy (see equation (4)) and therefore less energy has been deposited by the more energetic electrons, hence, the resist is less sensitive to exposure by the higher energy electrons.

Just for comparison, the equi-energy contours for the tri-level resist structure of Figure 10 and the Gallium-Arsenide case of Figure 9 are presented in Figures 20 and 21 respectively. Comparing these contours with those for the 0.5 μm of PMMA on silicon structure in Figure 17 the differences remarked upon earlier become clear. Looking at Figure 20 the resolution has obviously improved somewhat over the single-level structure and the problems of increased backscatter through using a more dense substrate are very well portrayed in Figure 21.

Figures 22-24 are another method of displaying the same data of Figures 16-18 and show the normalised energy dissipation distributions at the resist-substrate interface for the three resist thicknesses, 0.2, 0.5 and 1.0 microns. Figure 22 has been simulated with 20,000 50 keV electrons, Figure 23 with 20,000 20 keV electrons and Figure 24 with 20,000 10 keV electrons. The problem caused by backscattered electrons is quite evident in these diagrams. One notices that for the 20 keV and 10 keV case (Figures 23 and 24) there is a non-trivial amount of energy dissipated at one micron distant from the incident position, especially in the thicker resist. This will, in turn, cause inter-proximity effect between neighbouring features that are less than 1.0 microns apart. Further to these Figure 25 shows the dissipated energy distribution in 1.0 micron of PMMA on Silicon at five equi-spaced depths into the resist. Again we can see that even at the surface of the resist there is a background exposure that stretches out beyond 1.0 micron from the point of incidence and this will limit the maximum exposure contrast achievable.

The dissipated energy data can also be presented as three dimensional surfaces, as in Figures 26 to 30. Figures 26, 27 and 28 display the data of Figures 17 and 23 showing the energy deposited by a 20 keV electron beam of spot diameter of 0.2 microns in 1.0, 0.5 and 0.2 microns of PMMA on silicon respectively. Figures 29 and 30 show the energy deposited by a 50 keV and a 10 keV electron beam respectively, of spot diameter of 0.2 microns in 0.5 microns of PMMA on Silicon. These five figures are included to show the flexibility of the data achieved from the Monte Carlo simulations.

No energy data for the ion beam case is presented here because it is felt that secondary ion effects need to be taken account of before any serious exposure modelling can be attempted. The primaries trajectory plots were included to show the potential for high resolution lithography that focussed ion beams have.

4.3 LIMITATIONS OF THE MODEL

No account is made for the mechanism involved in the exposure of the polymer resist. Adesida et al[7] used Gryzinski's excitation function as a replacement for Bethe's continuous slowing down equation to try and model the exposing process more directly. They concluded that this approach gave a more realistic answer for the transmitted electron energy distribution. The effect of secondary electrons has been studied by Murata et al[8] and again they produced some slightly different results. The main effect was a broadening of the energy distribution, especially towards the surface of the resist. However, it was considered that the difference these adjustments made to the overall results did not warrant the increased complexity in the models as this is primarily a study of the lithographic process and is not an in-depth study of particle scattering in solids. A further limitation,

within the Monte Carlo method, is that both substrate and resist are assumed to be totally amorphous. This will probably have a bigger effect on the electron case than the ion because any channelling due to the crystalline structure will effect the backscatter and we expect zero, or very nearly, backscatter of the ions. However, we are only interested in the energy deposited into the amorphous resist layer in this application, thus channelling is of little direct relevance.

The Monte Carlo method has a few practical disadvantages such as the need for a large computer and hours of CPU time to simulate a large number of electrons in order to smooth out the statistical fluctuations. Also the data is returned in histogram form instead of analytical form. However, these problems can be tolerated because the model is fairly simple and each run of the programme returns enough information that it need only be done once for each substrate and resist parameters. This data can then be manipulated further for changes in other conditions, like beam spot size, afterwards.

5 CONCLUSIONS

The Monte Carlo method of simulating scattering and energy loss by energetic particles incident upon resist-substrate structures has been investigated as a means to understanding the exposure of resist polymers in particle beam lithography.

The results presented clearly show the problem of backscattered electrons limiting the resolution capabilities of electron beam lithography and suggest that improvements can be made by reducing the thickness of the resist layer employed and by using higher energy electrons. The trajectory plots of the primary ions show that ion beam lithography is limited only by the small amount of forward scattering experienced by the ions and, therefore, has the potential for high resolution.

The models used in this study are comparatively simple yet very powerful and are able to indicate the roots of many problems, such as proximity effect, experienced by electron beam lithographers. The models can be used to investigate viable solutions to these problems and to predict performance on new substrates and new resist structures.

6 FUTURE WORK

The work presented here is currently being expanded to include simulations of other processes within the lithographic system to improve the predictive power of the simulations. The extensions to be included are:

i. Simulation of shaped beam systems. This is a very simple modification to the present system. All that is required is that the data produced by the Monte Carlo simulation be convoluted with the appropriate beam shape required (see section 3.3).

ii. Inclusion of secondary ion effects. As mentioned in section 4.2 secondary ions are considered to play an important role in exposure by ion beams. Therefore, these will be included in the simulations for ion beam exposures.

iii. Development modelling. To complete the modelling suite multi-pass exposures of features in resist and their realisation by development are to be simulated. This will provide the capability of being able to produce theoretical features to compare with those we gain from our experimental programme.

REFERENCES

1 Bishop, H E; Brit J Appl Phys 18, 703 (1967).

2 Shimizu, R and Murata, K; J Appl Phys 42, 387 (1971).

3 Murata, K; Matsukawa, T and Shimizu, R; Jap J Appl Phys 10, 678 (1971).

4 Kyser, D F and Murata, K; IBM J Res and Develop 18, 350 (1974).

5 Shimizu, R; Ikuta, T; Everhart, T E and Devore, W J; J Appl Phys 46, 1581 (1975).

6 Kyser, D F and Murata, K; Proc 6th Int Conf Electron and Ion Beam Sci Technol (Ed. R Bakish), pp205-223 (1974).

7 Adesida, I; Shimizu, R and Everhart, T E; Appl Phys Lett 33(10), 849, (1978).

8 Murata, K; Kyser, D F and Ting, C H; J Appl Phys 52(7), 4396 (1981).

9 Robinson, M T and Torrens, I M; Phys Rev B9, 5008 (1974).

10 Biersack, J P and Haggmark, L G; Nucl Instr and Meth 174, 257 (1980).

11 Adesida, I and Karapiperis, L; Radiat Eff 61, 223 (1982).

12 Karapiperis, L; Adesida, I; Lee, C A and Wolf, E D; J Vac Sci Technol 19(4), 1259 (1984).

13 Kalbitzer, S and Oetzmann, H; Radiat Eff 47, 57 (1980).

14 Lindhard, J; Scharff, M and Schiott, H E; Mat Fys Medd Dan Vid Selsk 33(14) (1963).

15 Phang, J C H; PhD Thesis, Cambridge University, 1979, Ch2 (unpublished).

16 Anderson, H H and Zeigler, J F; "Hydrogen Stopping Power and Ranges in all Elements", (Pergamon Press, New York, 1977), Vol 3.

17 Dearnaly, G; Freeman, J H; Nelson, R S and Stephen, J; "Ion Implantation", Vol 8 of series "Defects in Crystalline Solids", (North-Holland Publishing Company, 1973).

18 Schiott, H E; Matt Fys Medd Dan Vid Selsk 35, 9 (1966).

19 Cosslett, V E and Thomas, R N; Brit J Appl Phys 15, 235 (1964).

20 Oen, O S and Robinson, M T; J Nucl Mater 76 & 77, 370 (1978).

21 Parikh, M and Kyser, D F; J Appl Phys 50(2), 1104 (1979).

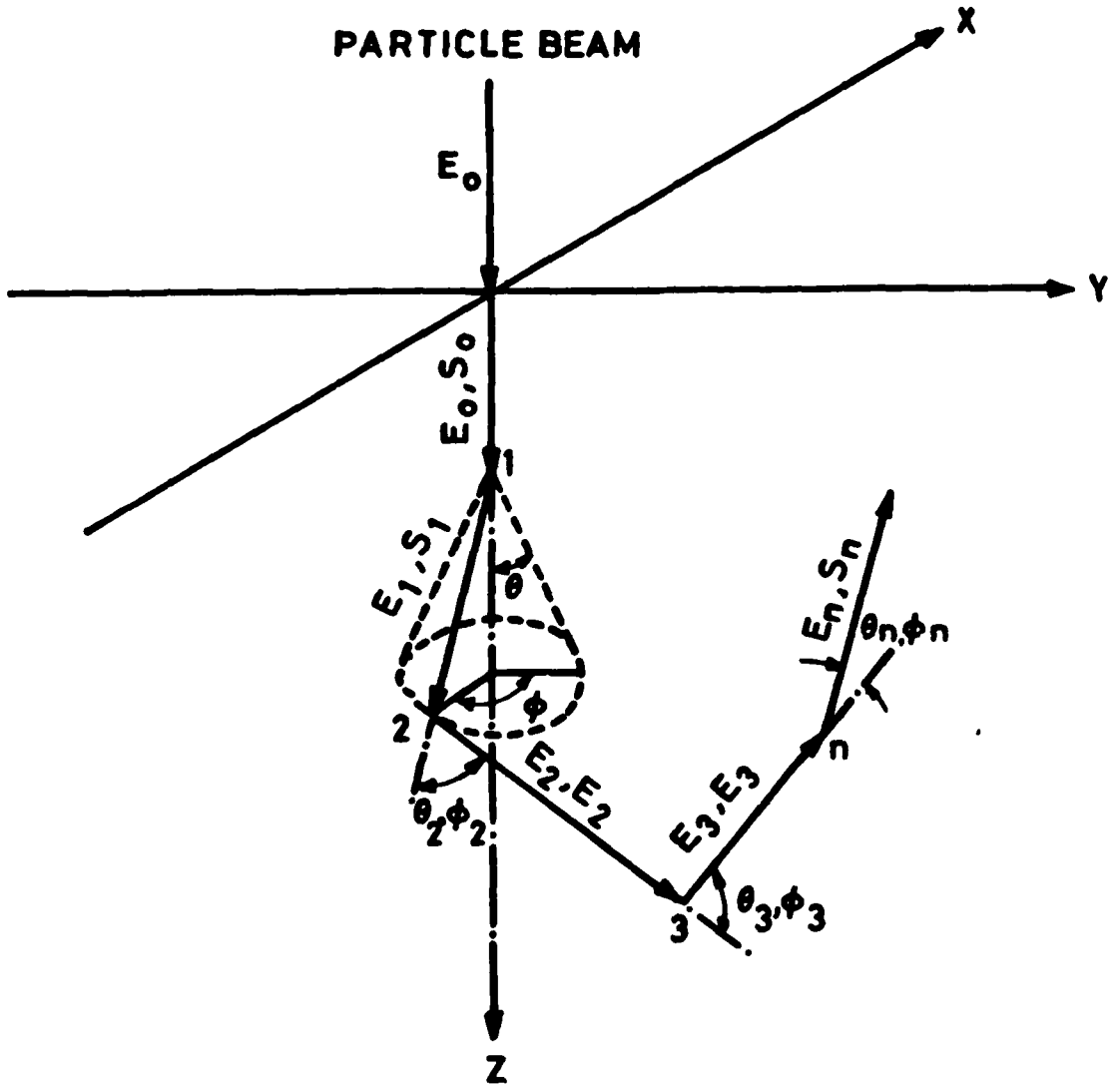

Figure 1. Geometry for Monte carlo simulations.

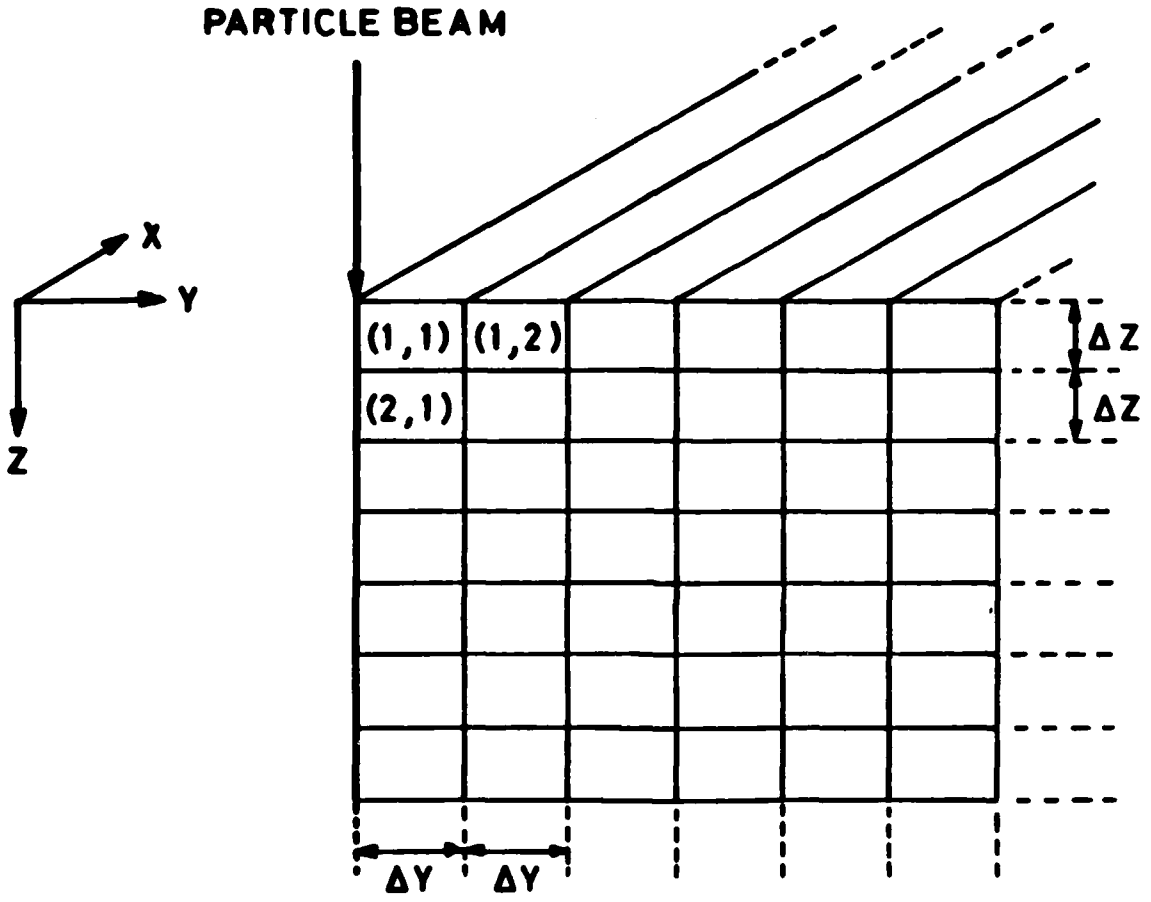

Figure 2. Parallelapipeds used for calculating energy dissipation.

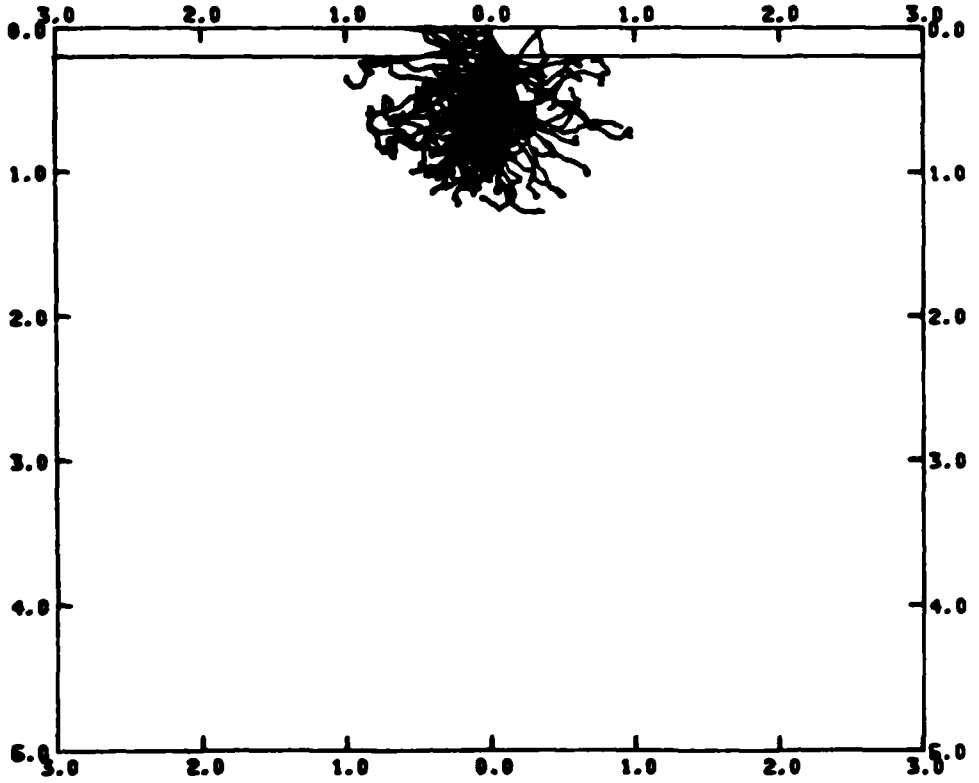

Figure 3. Simulated trajoctories of 100 electrons at 10 keV incident upon 0.2 um of PMMA on a silicon substrate.

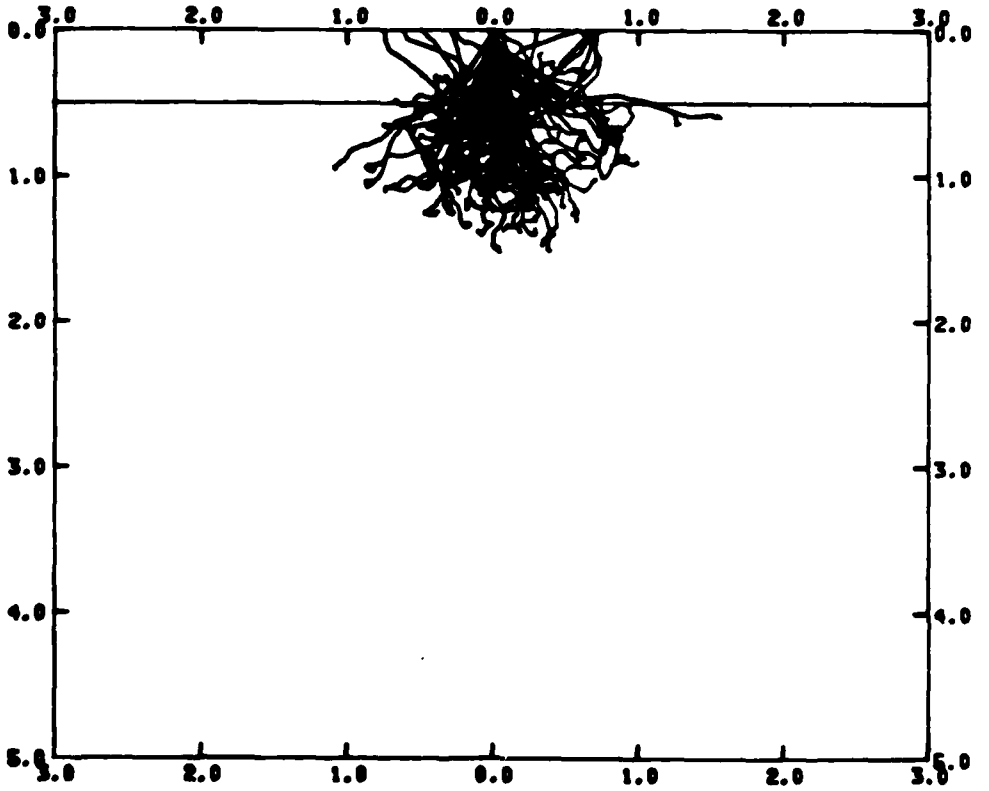

Figure 4. Simulated trajoctories of 100 electrons at 10 keV incident upon 0.5 um of PMMA on a

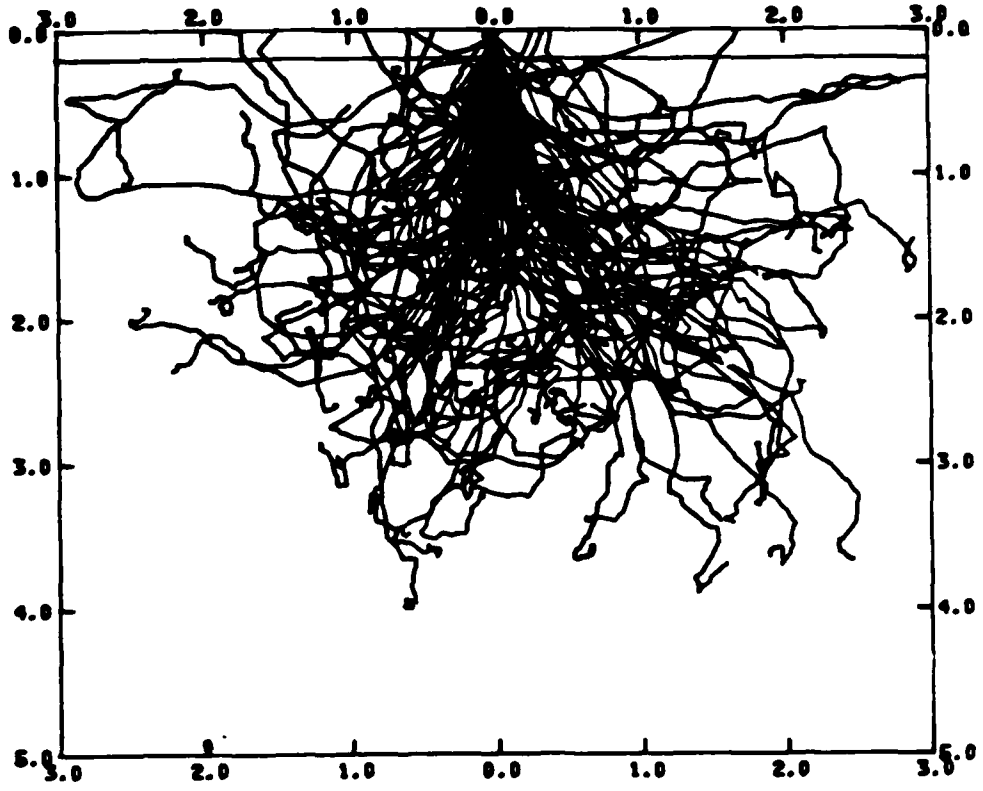

Figure 5. Simulated trajoctories of 100 electrons at 20 keV incident upon 0.2 um of PMMA on a silicon substrate.

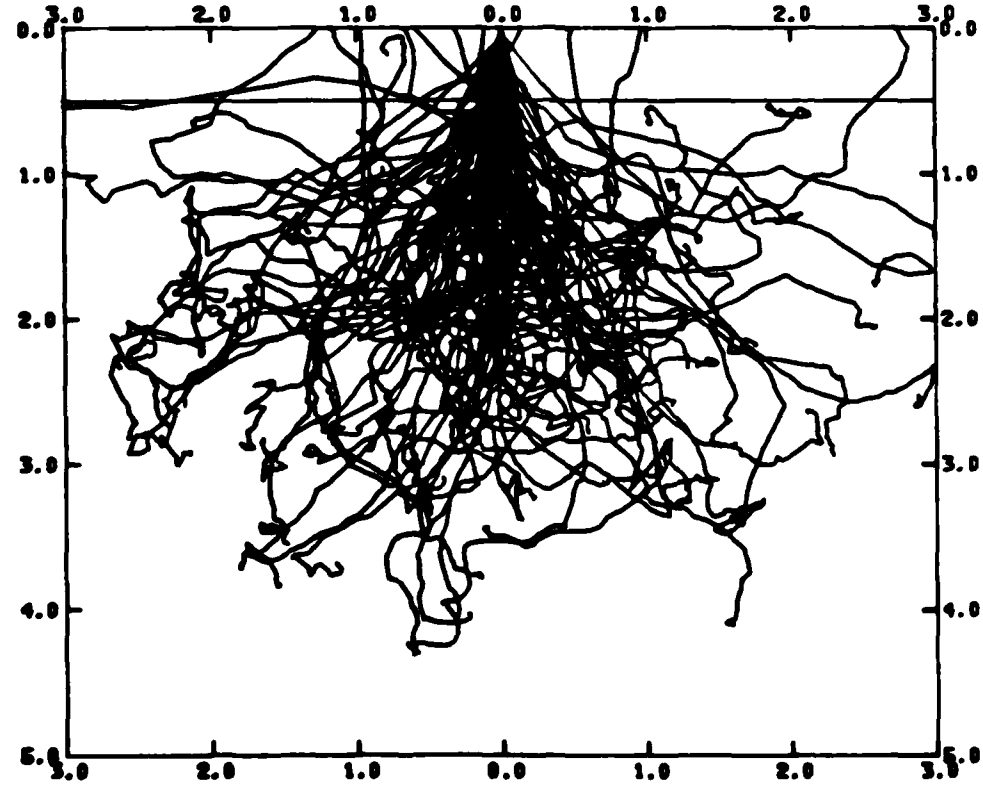

Figure 6. Simulated trajoctories of 100 electrons at 20 keV incident upon 0.5 um of PMMA on a

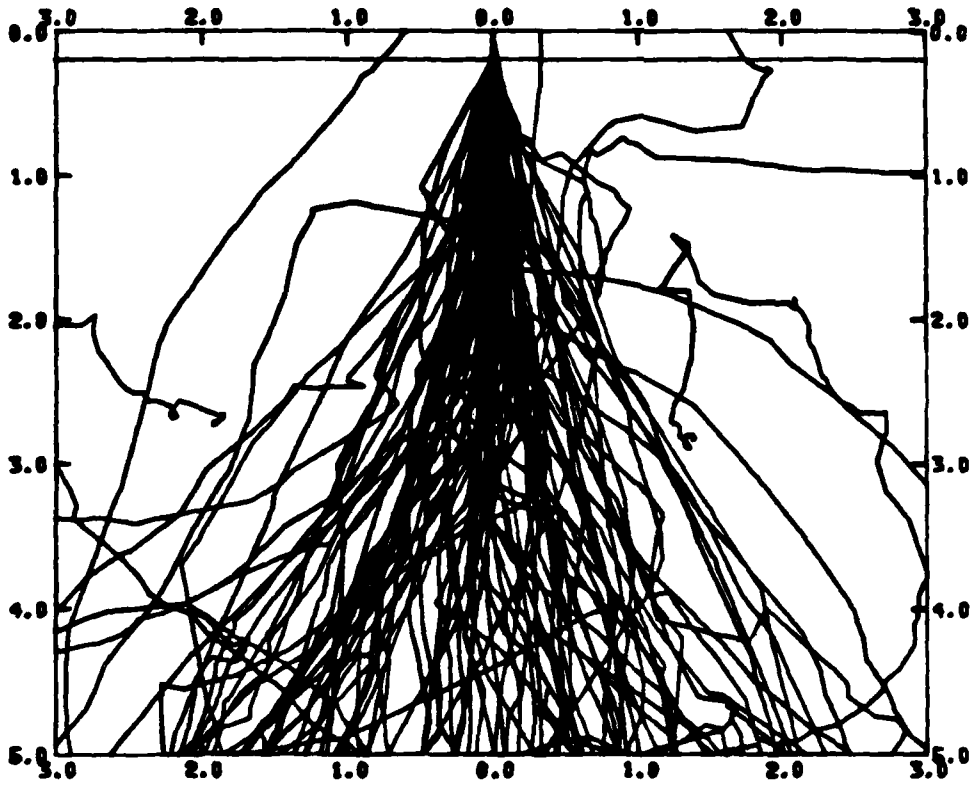

Figure 7. Simulated trajoctories of 100 electrons at 50 keV incident upon 0.2 um of PMMA on a silicon substrate.

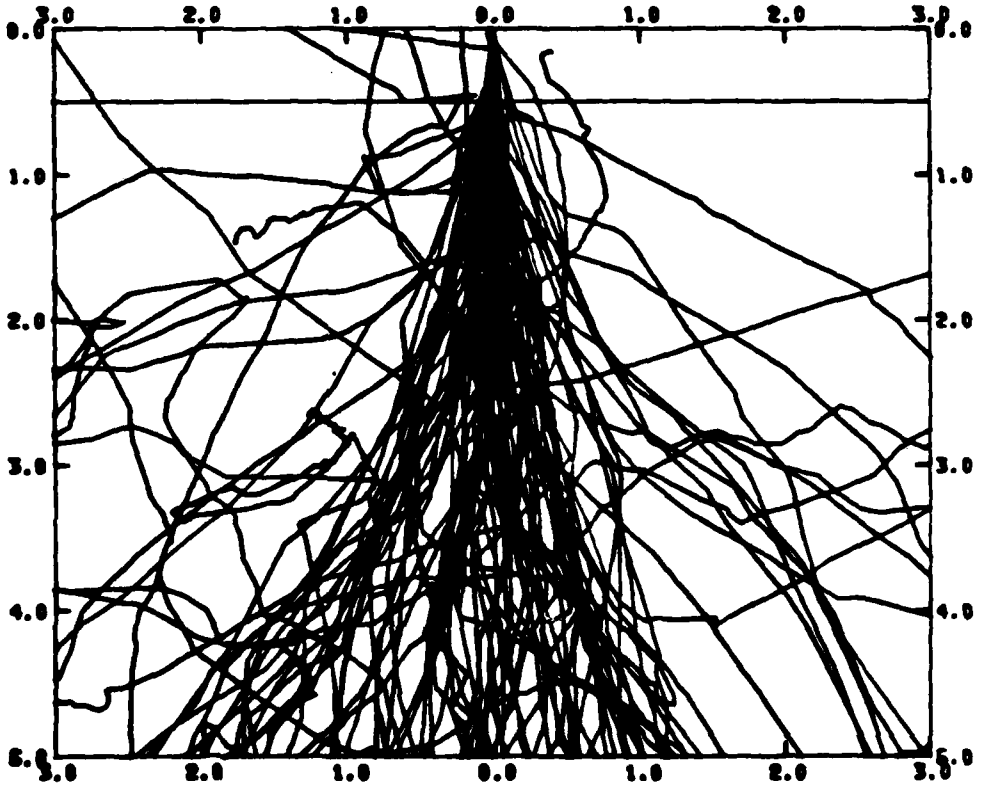

Figure 8. Simulated trajoctories of 100 electrons at 50 keV incident upon 0.2 um of PMMA on a

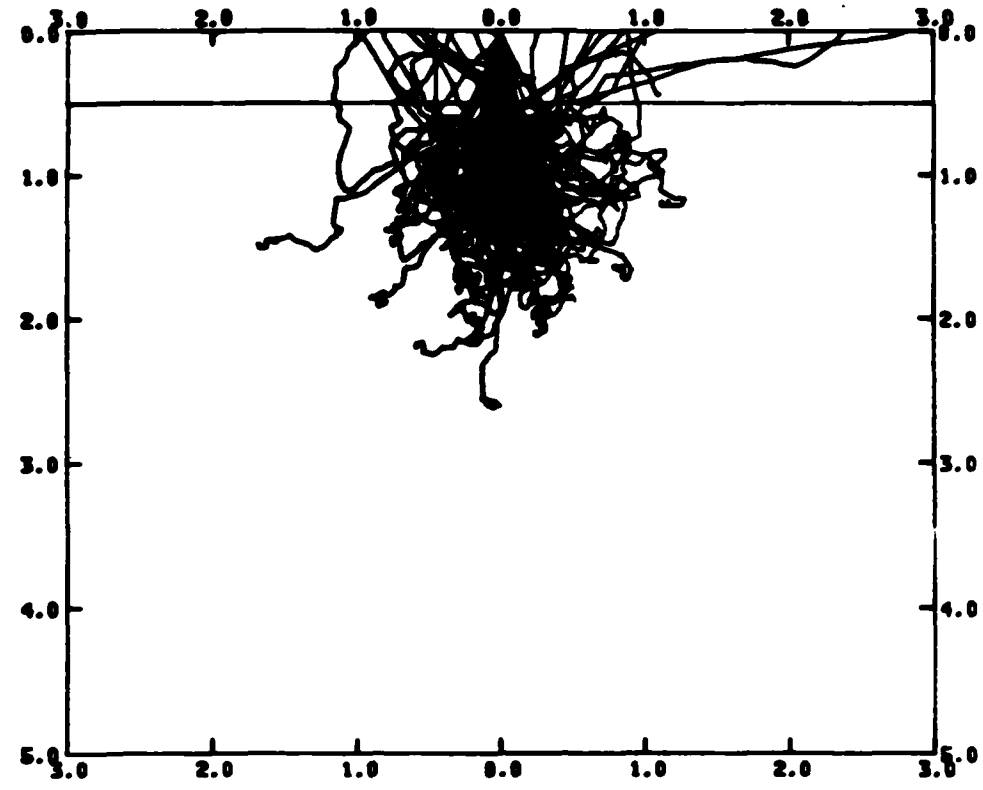

Figure 9. Simulated trajectories of 100 electrons at 20 keV incident upon 0.5 um of PMMA on Gallium Arsenide

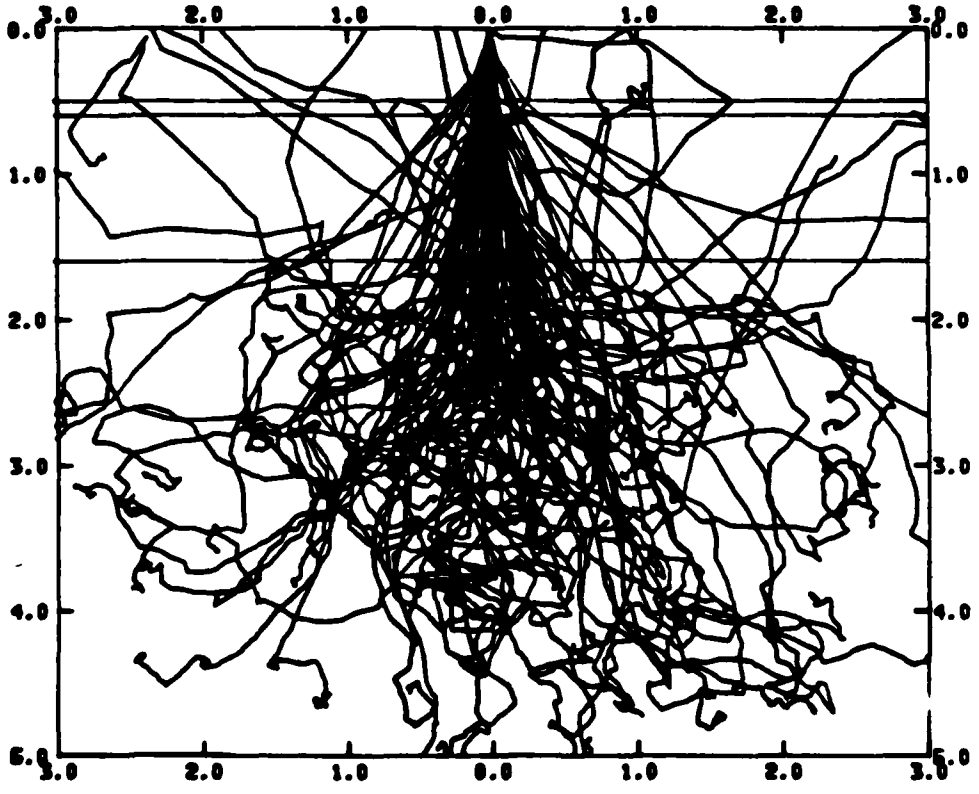

Figure 10. Simulated trajectories of 100 electrons at 20 keV incident upon a tri-level resist structure consisting of

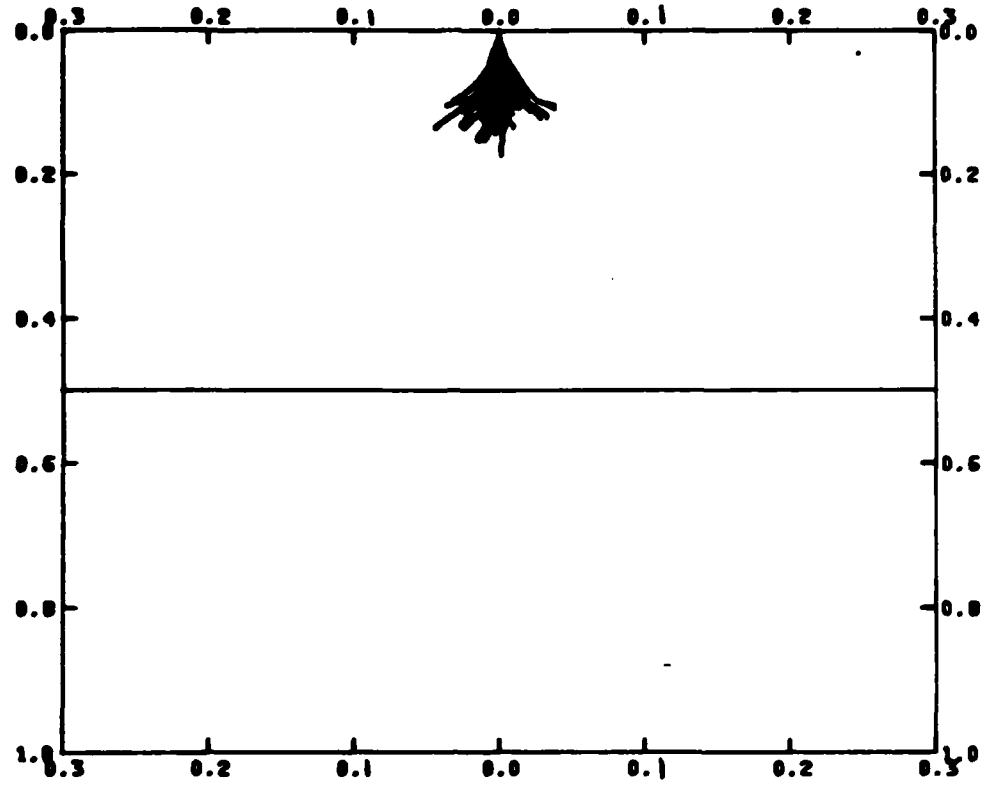

Figure 11. Simulated trajectories of 50 100keV Gallium ions incident upon 0.5 microns of PMMA on a silicon substrate.

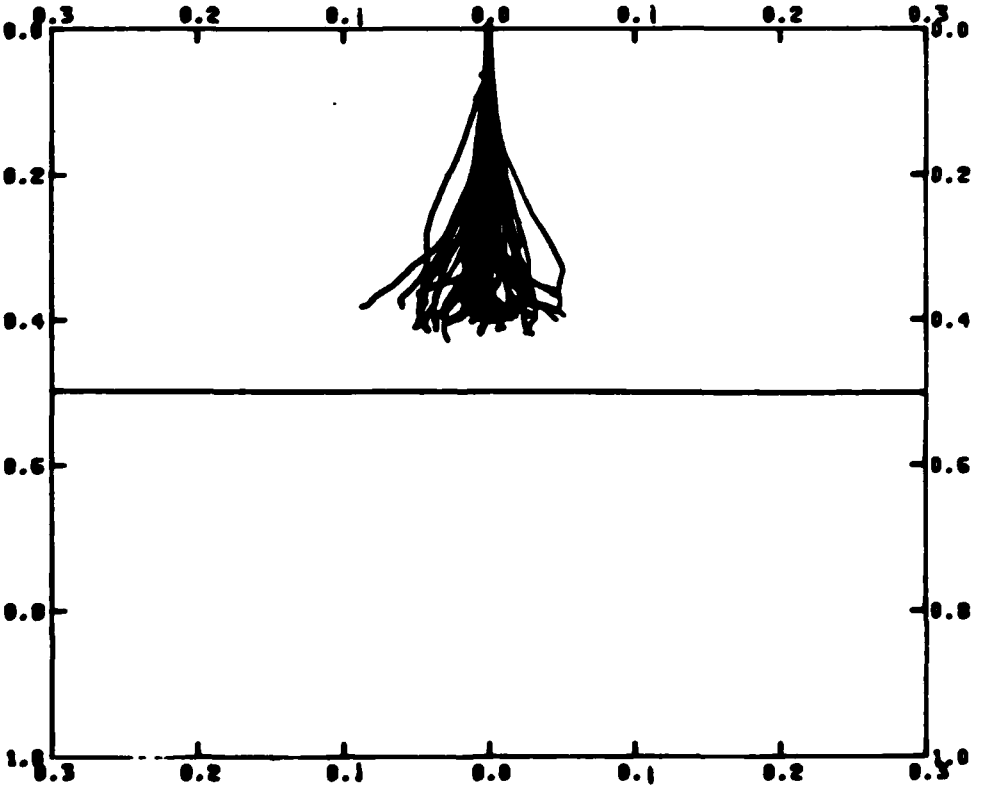

Figure 12. Simulated trajectories of 50 200keV silicon ions incident upon 0.5 microns of PMMA on a silicon substrate.

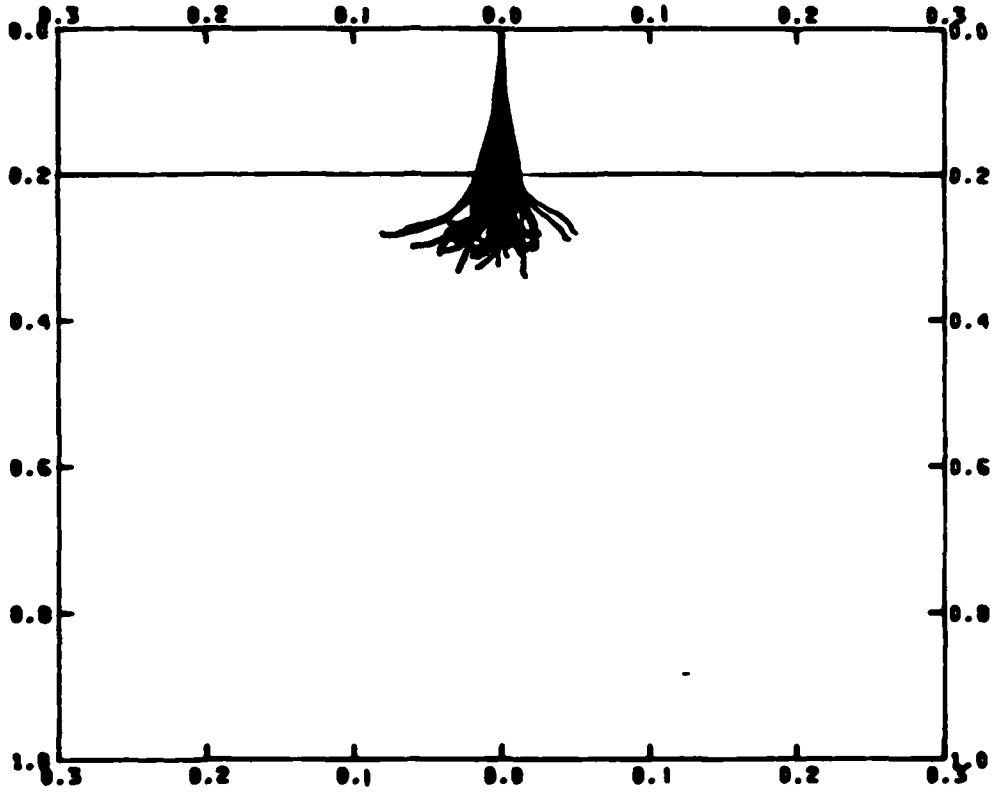

Figure 13. Simulated trajectories of 50 200keV silicon ions incident upon 0.2 microns of PMMA on a silicon substrate.

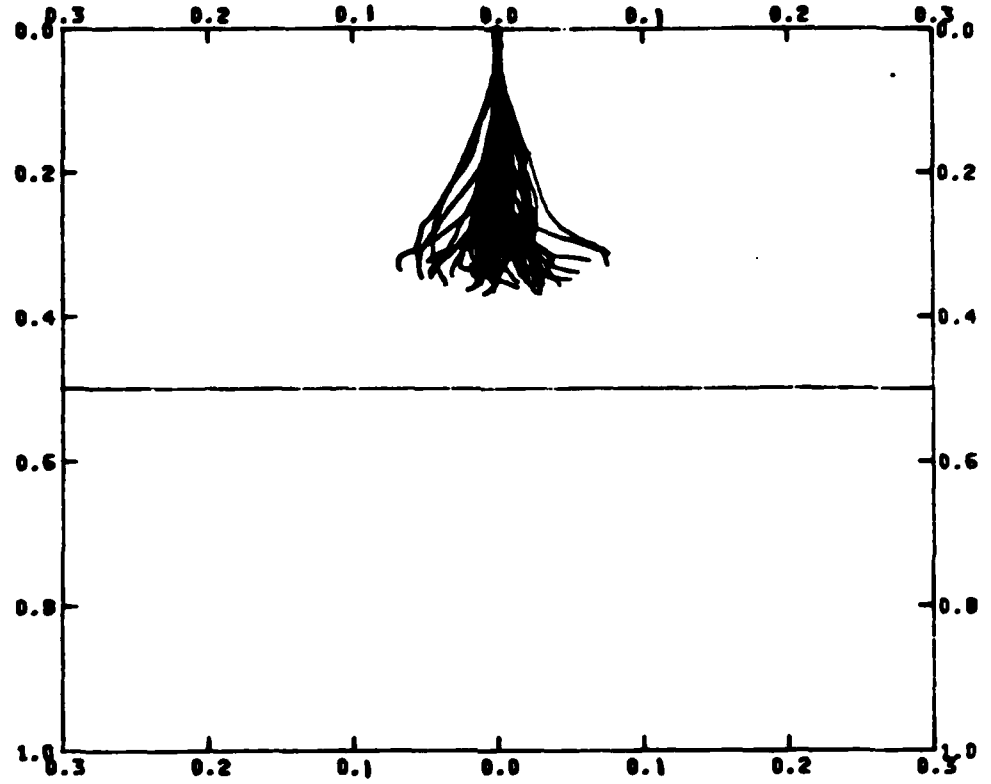

Figure 14. Simulated trajectories of 50 150keV silicon ions incident upon 0.5 microns of PMMA on a silicon substrate.

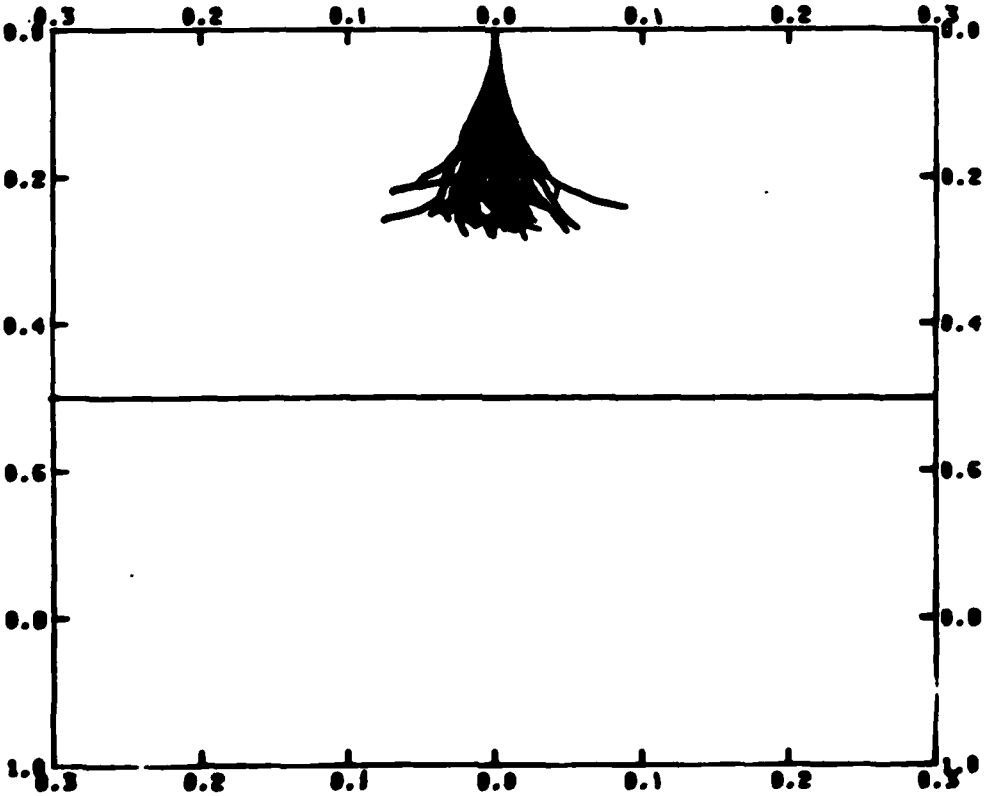

Figure 15. Simulated trajectories of 50 100keV silicon ions incident upon 0.5 microns of PMMA on a

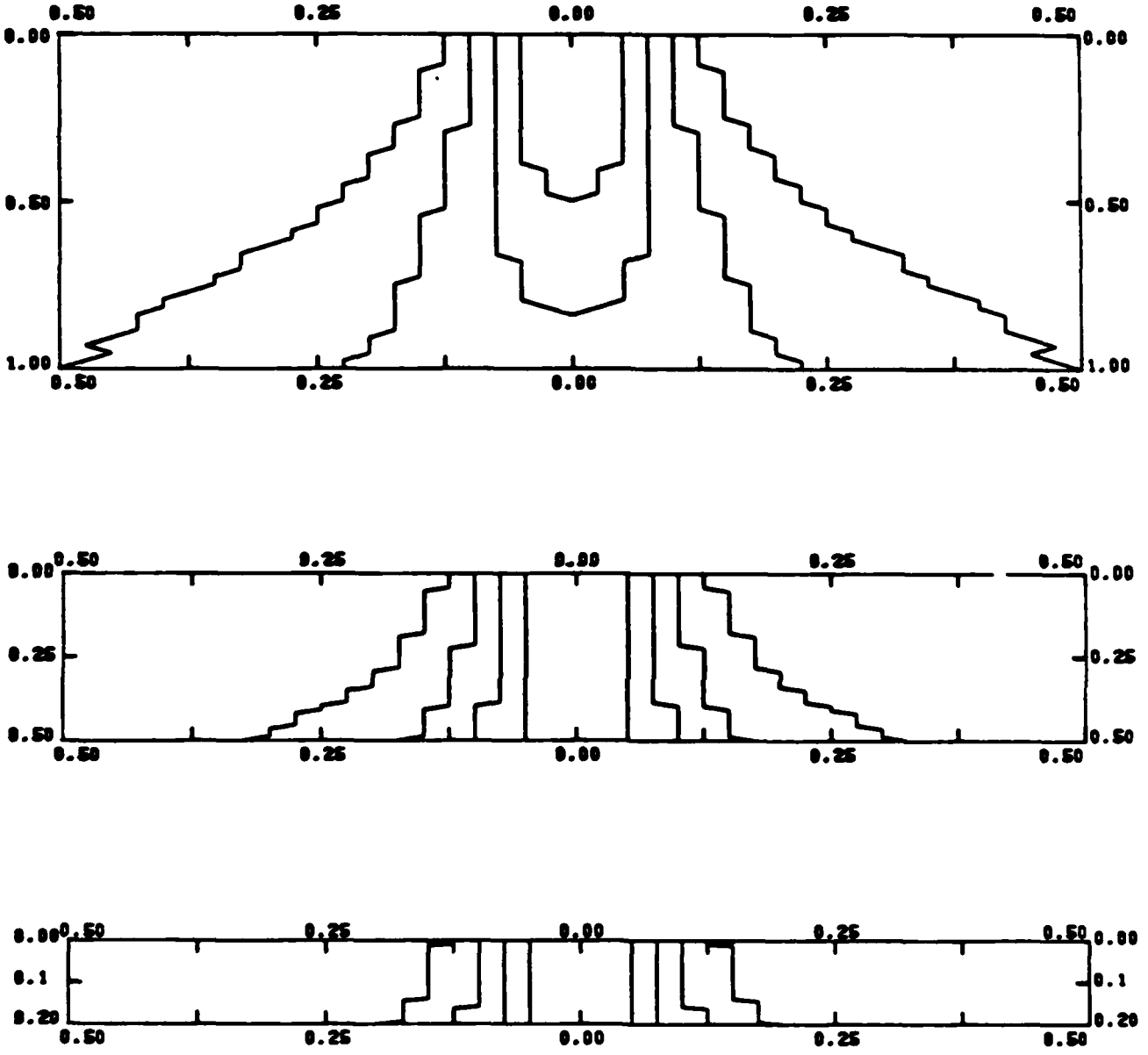

Figure 16. Equi-energy contours simulated with 20000 10 keV electrons. The energy levels are abitrary but consistent through the three diagrams.

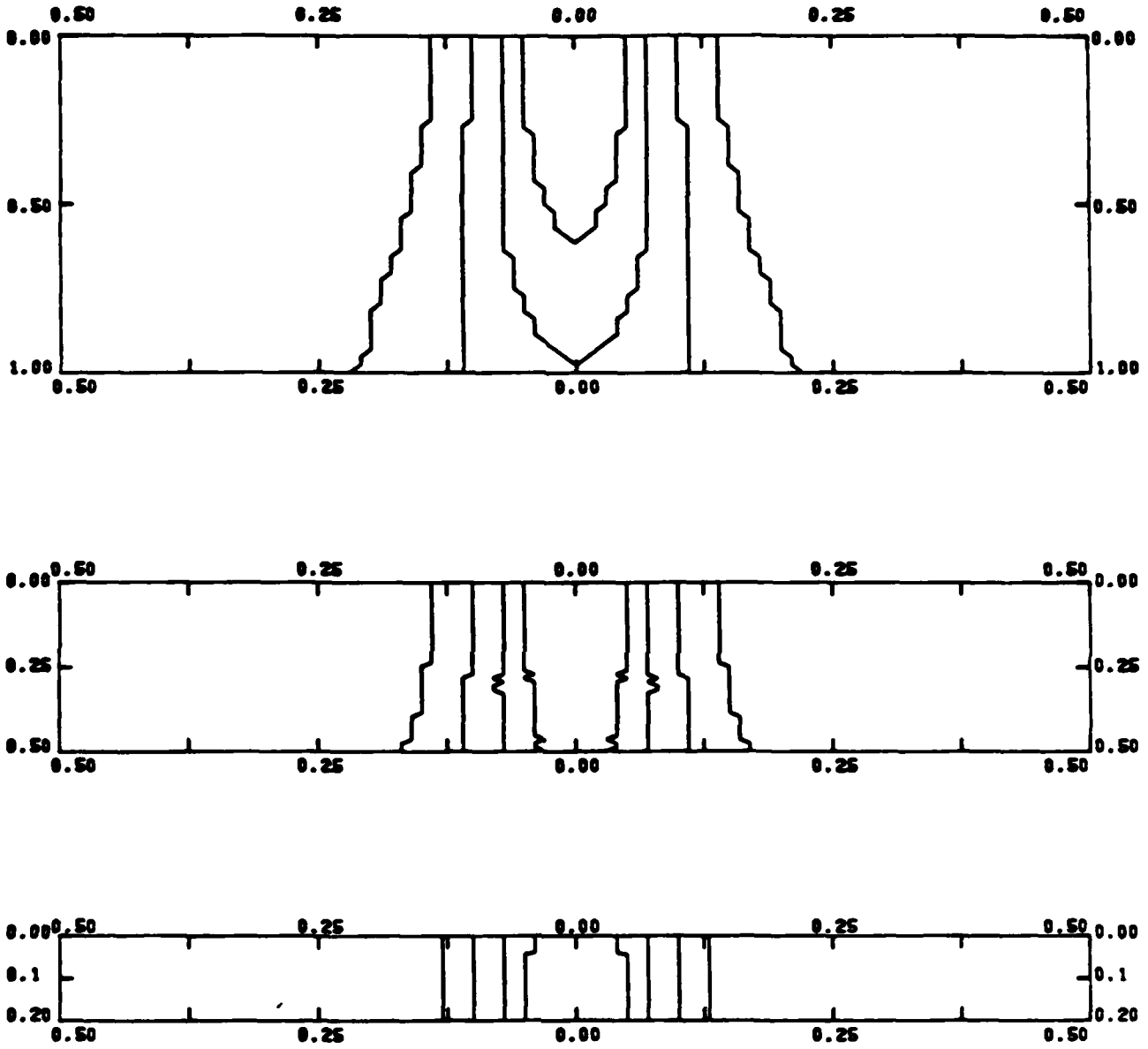

Figure 17. Equi-energy contours simulated with 20000 20 keV electrons. The energy levels are abitrary but consistent through the three diagrams.

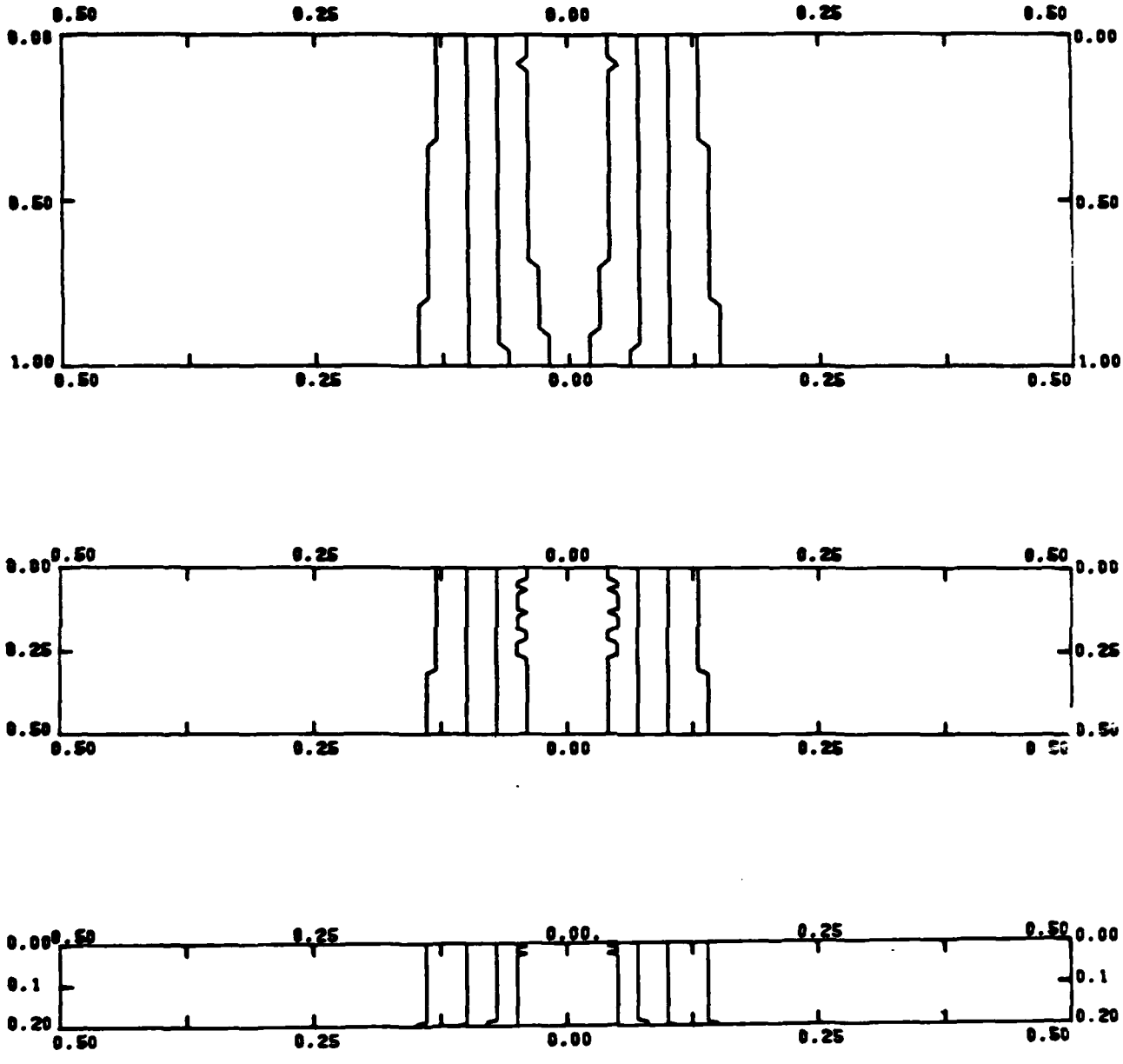

Figure 18. Equi-energy contours simulated with 20000 50 keV electrons. The energy levels are abitrary but consistent through the three diagrams.

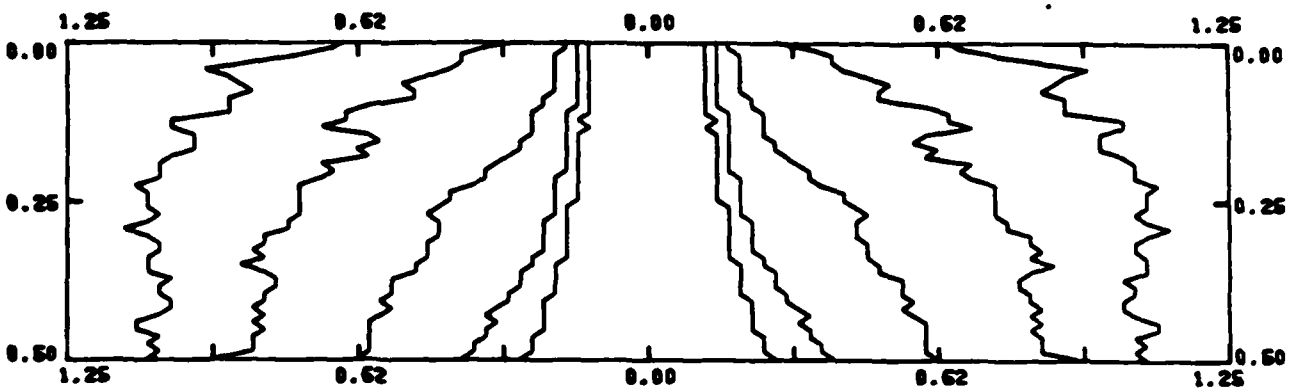

a) 10 keV

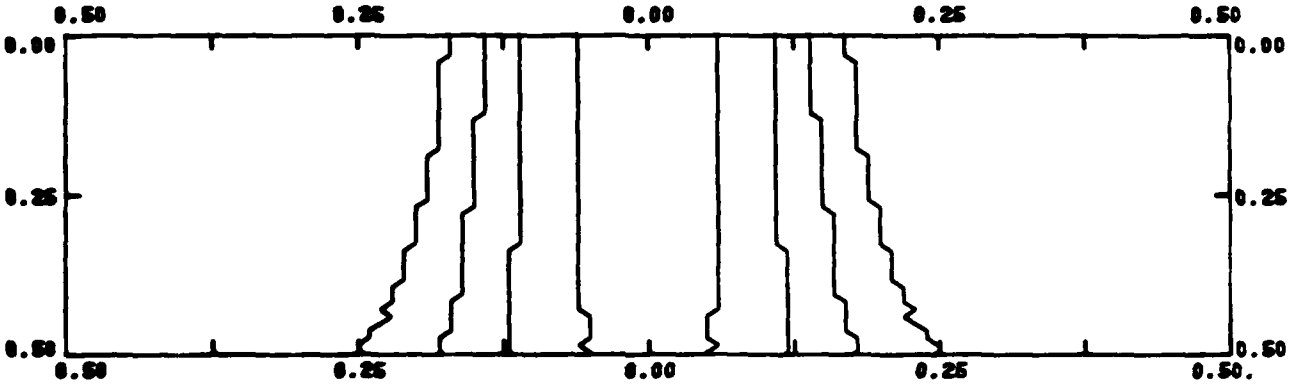

b) 20 keV

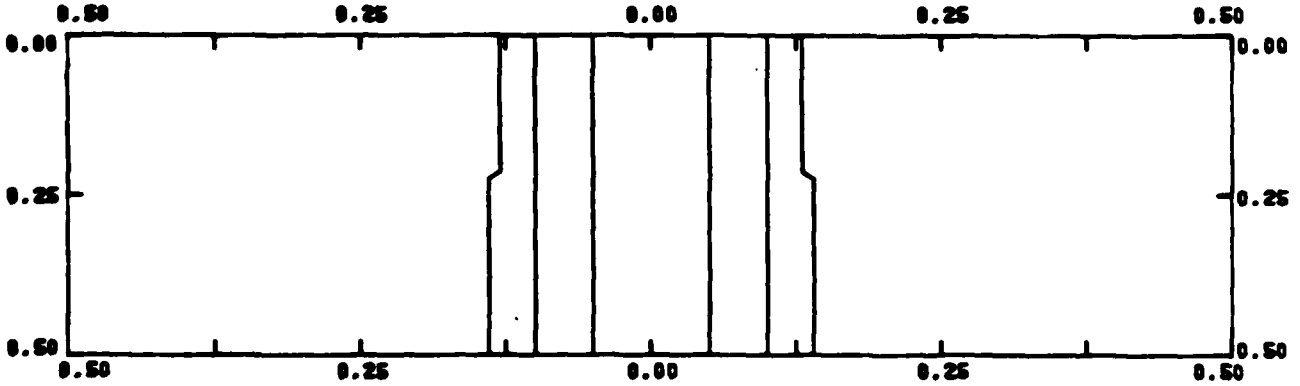

c) 50 keV

Figure 19. Equi-energy levels within a 0.5 micron layer of PMMA after being exposed by 20000 electrons at an incident energy of a)10 keV, b)20 keV & c)50 keV. The energy levels are abitrary but consistent through the three diagrams.

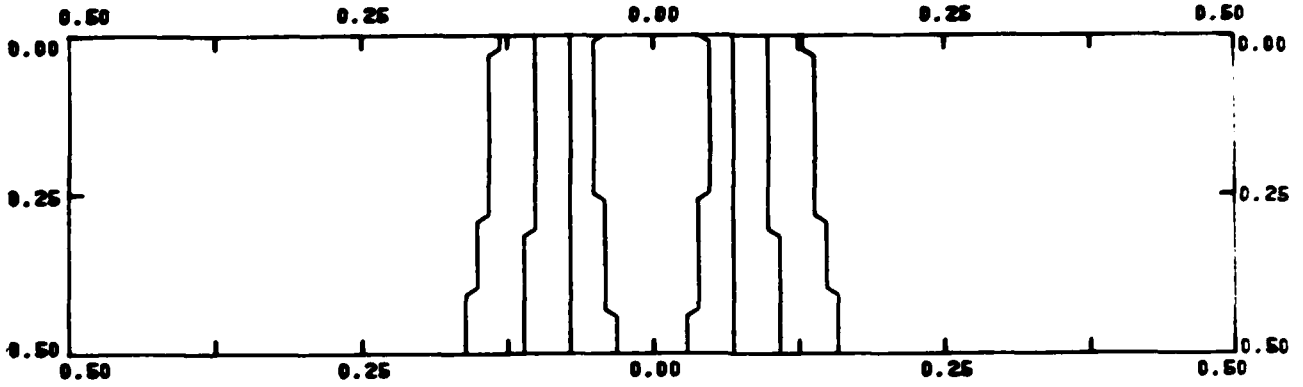

Figure 20. Equi-energy contours within the top resist layer of the tri level resist structure of figure 10. Simulated with 20000 20 kev electrons

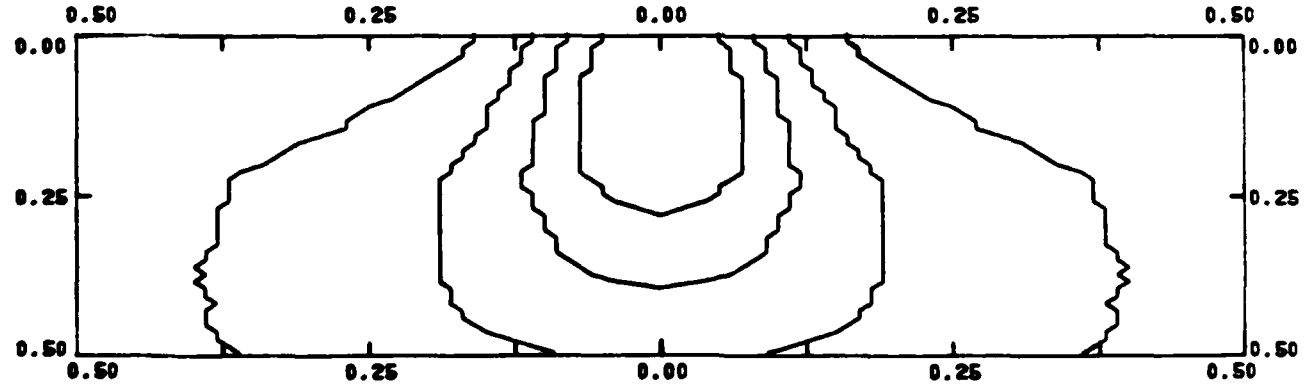

Figure 21. Equi-energy contours simulated with 20000 20 keV electrons into 0.5 um of PMMA resist on a Gallium-Arsenide substrate.

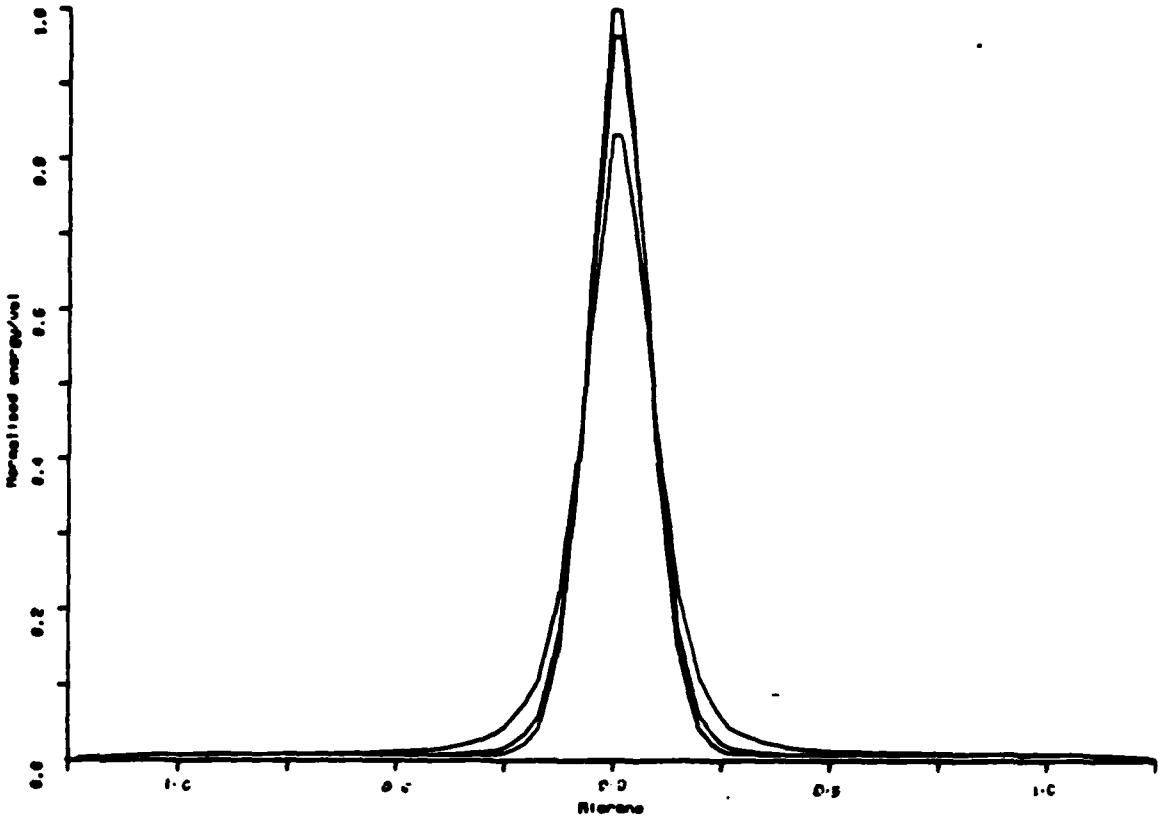

Figure 22. Distribution of energy dissipated per unit volume at resist/substrate interface by 50 keV electrons in three thicknesses of PMMA resist.

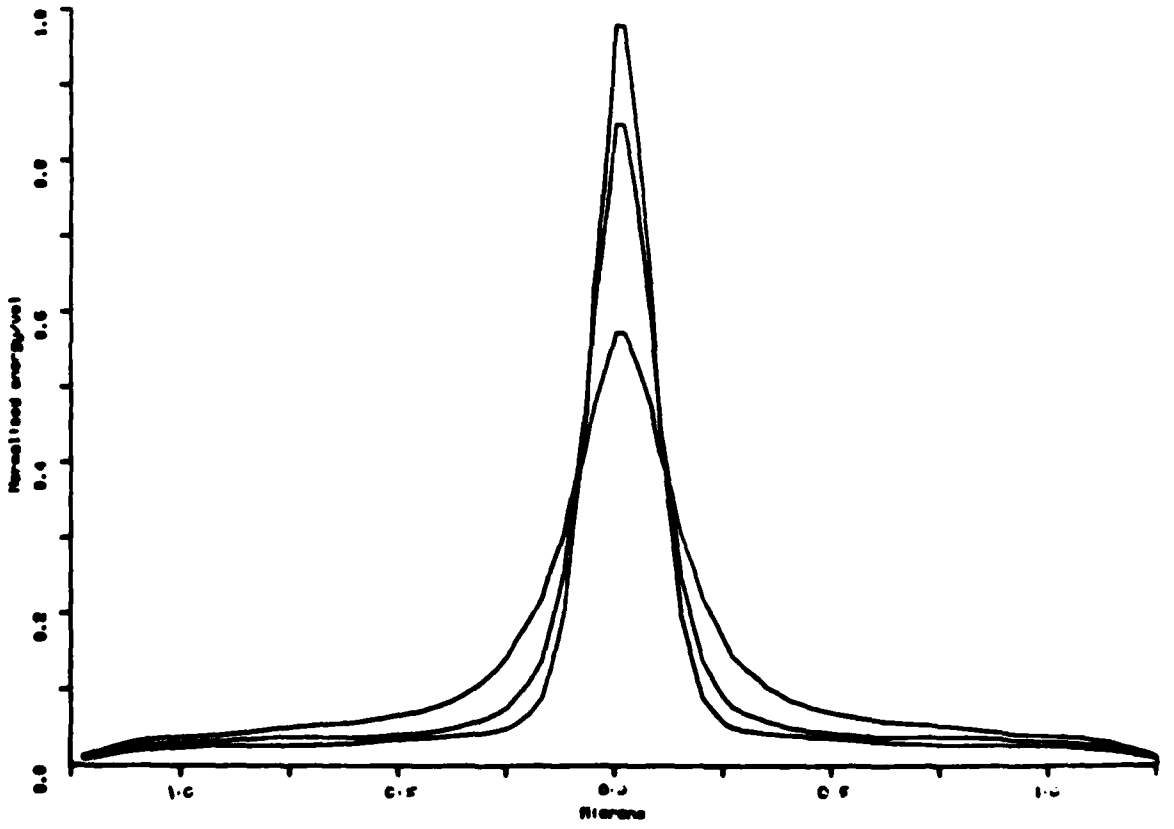

Figure 23. Distribution of energy dissipated per unit volume

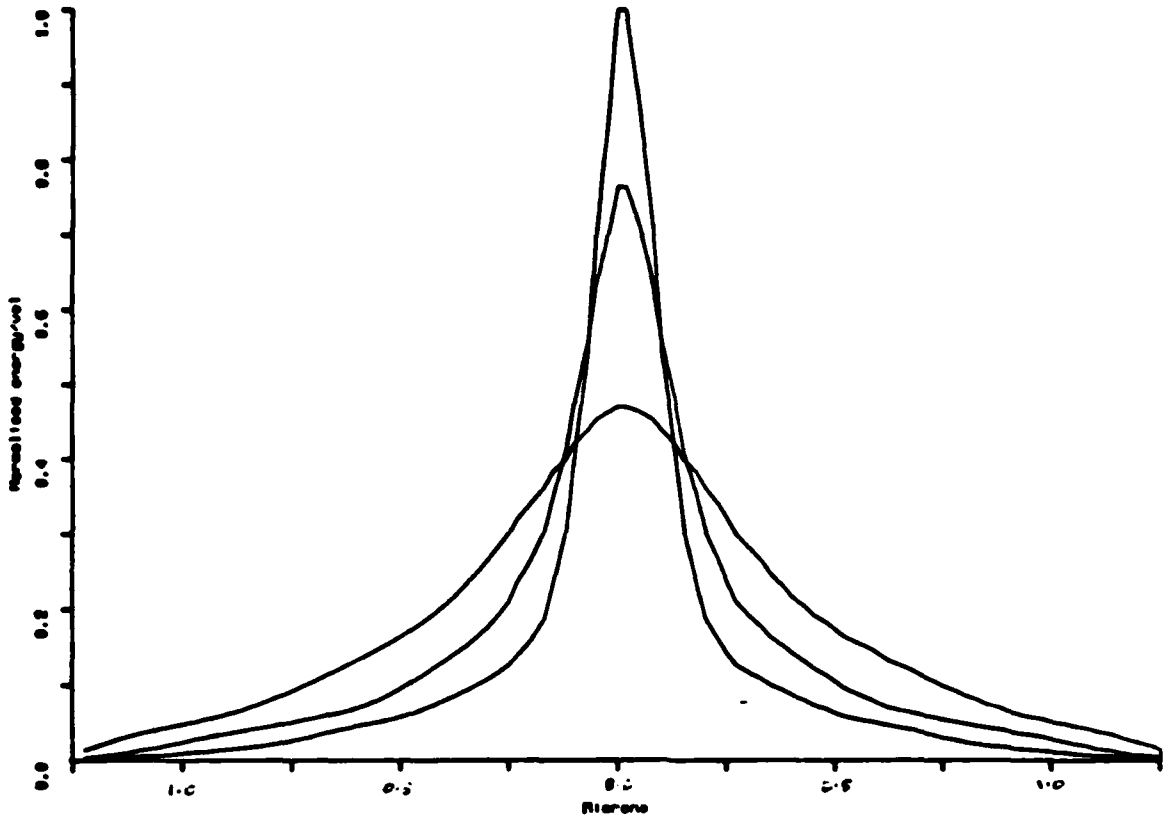

Figure 24. Distribution of energy dissipated per unit volume at resist/substrate interface by 10 keV electrons in three thicknesses of PMMA resist.

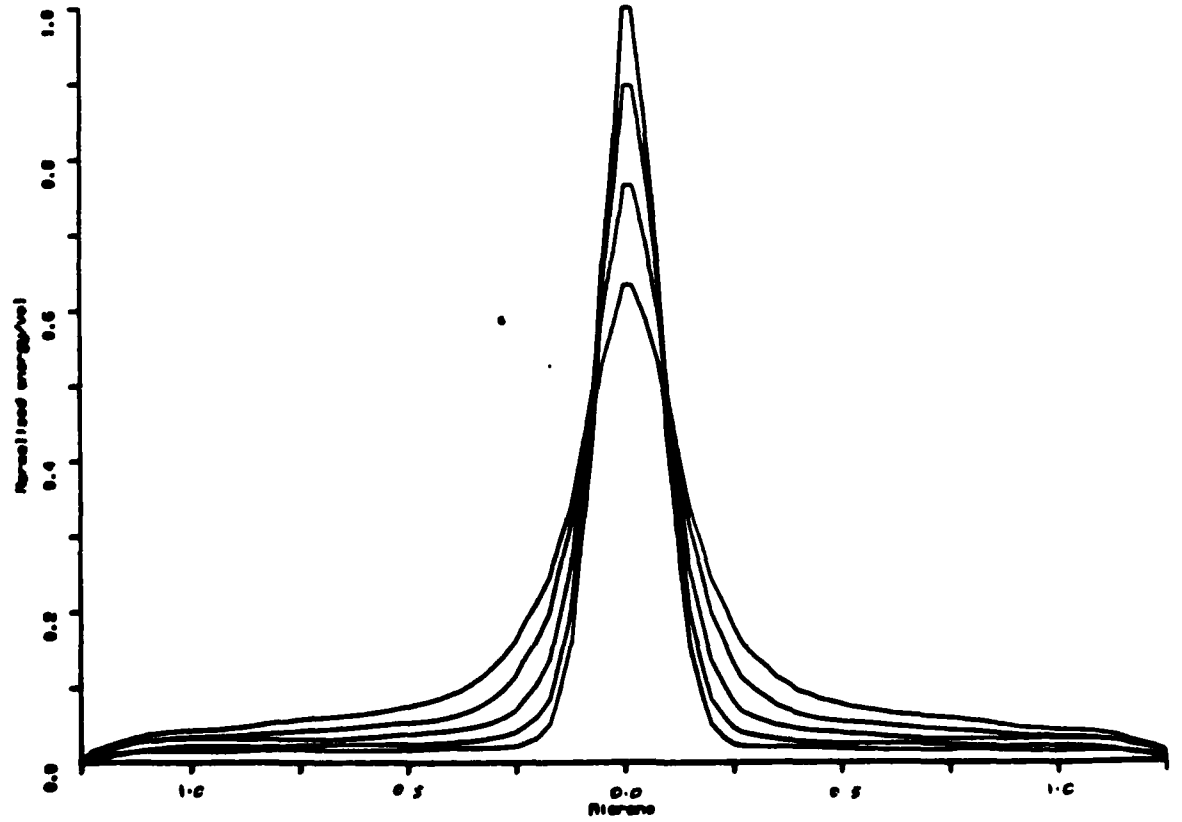

Figure 25. Distribution of energy dissipated per unit volume

Scale (Y:Z)

0.50 um : 1.11 um

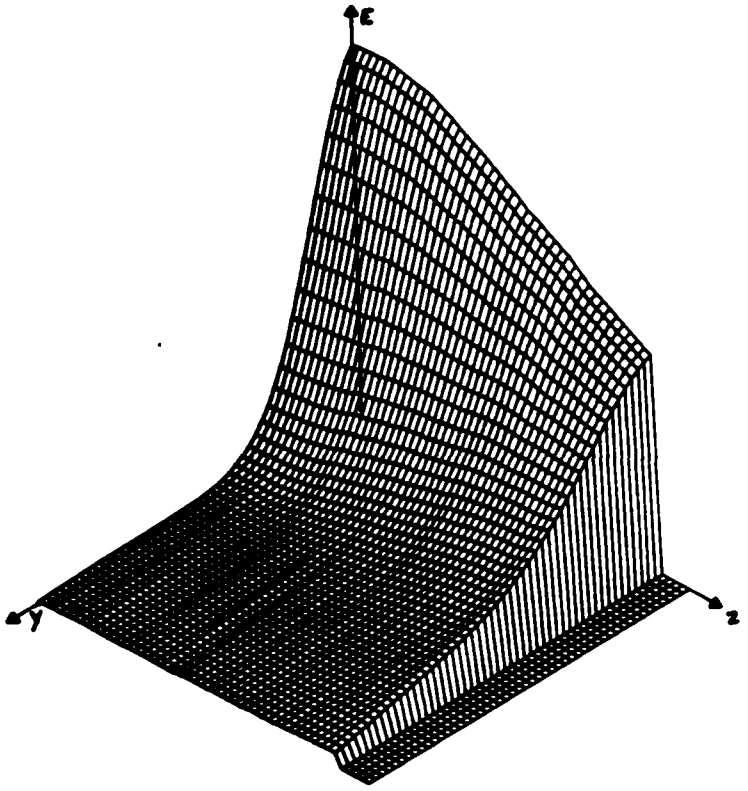

Figure 26. Energy deposition surface simulated with a 0.2 um beam of 20 keV electrons incident upon 1.0 um of PMMA on Silicon.

Scale (Y:Z)

0.50 um : 0.56 um

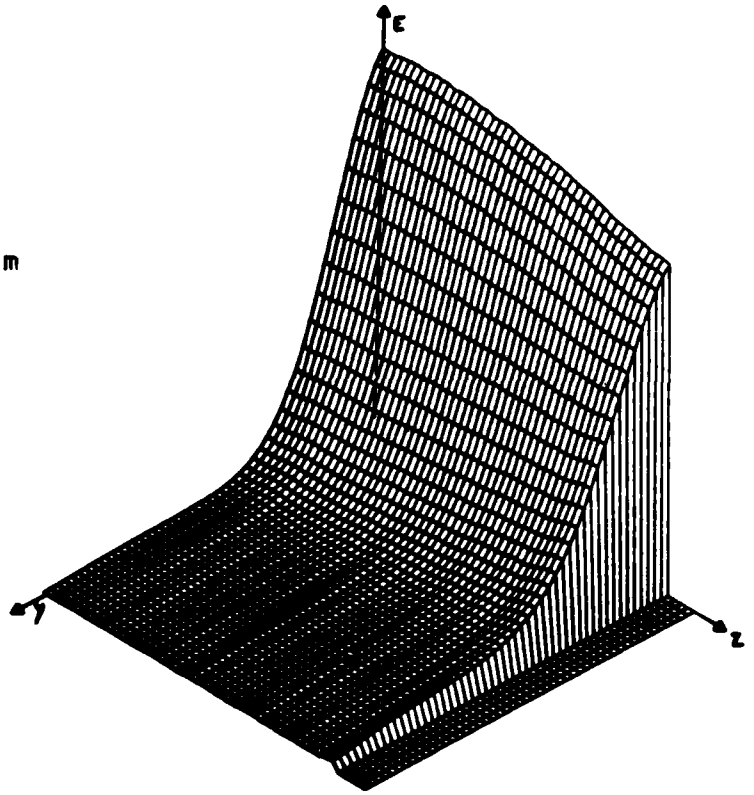

Figure 27. Energy deposition surface simulated with a 0.2 um beam of 20 keV electrons incident upon

Scale (Y:Z)

0.50 um : 0.22 um

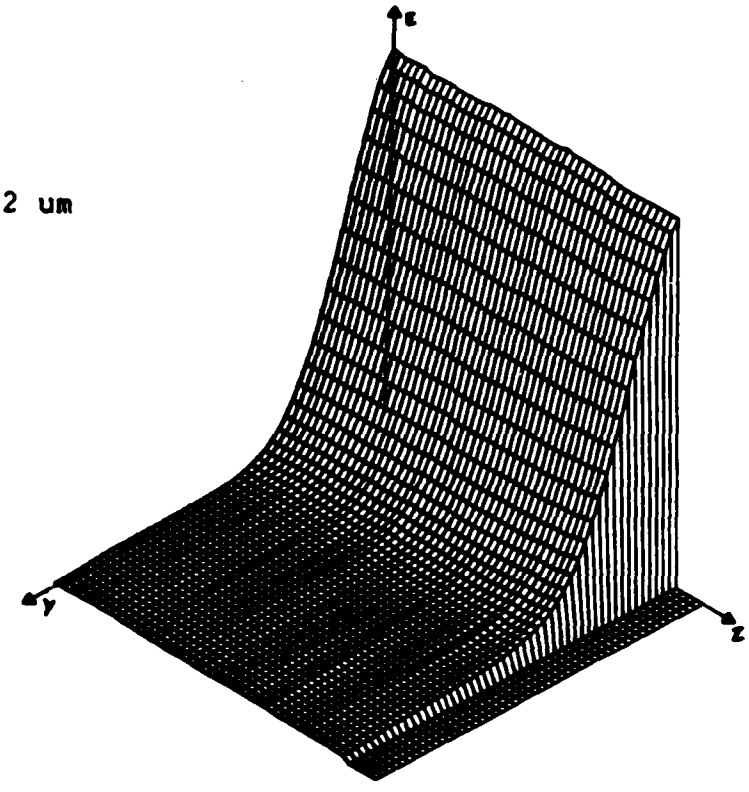

Figure 28. Energy deposition surface simulated with a 0.2 um beam of 20 keV electrons incident upon 0.2 um of PMMA on Silicon.

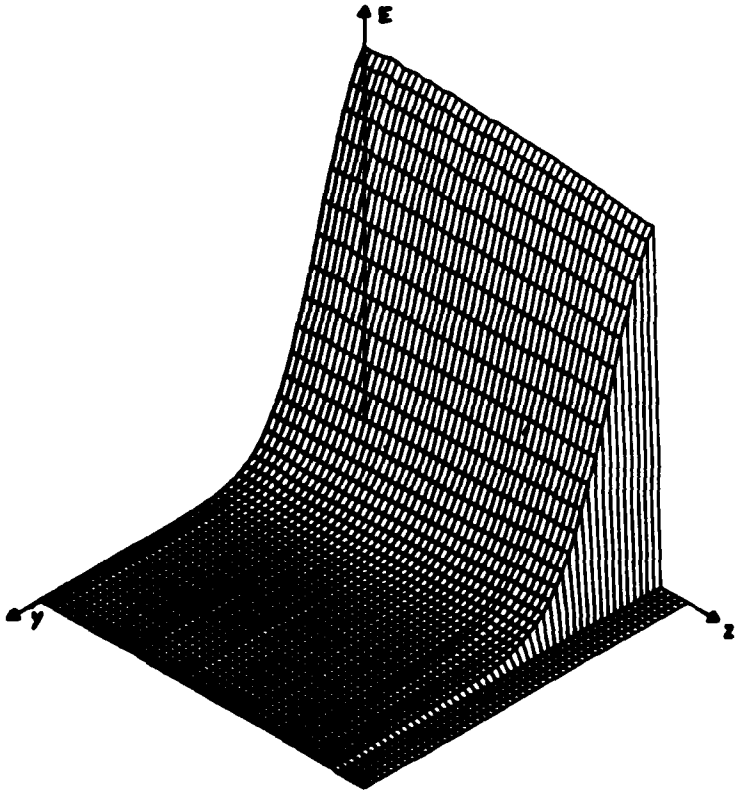

Scale (Y:Z)

0.50 um : 0.56 um

Figure 29. Energy deposition surface simulated with a 0.2 um beam of 50 keV electrons incident upon

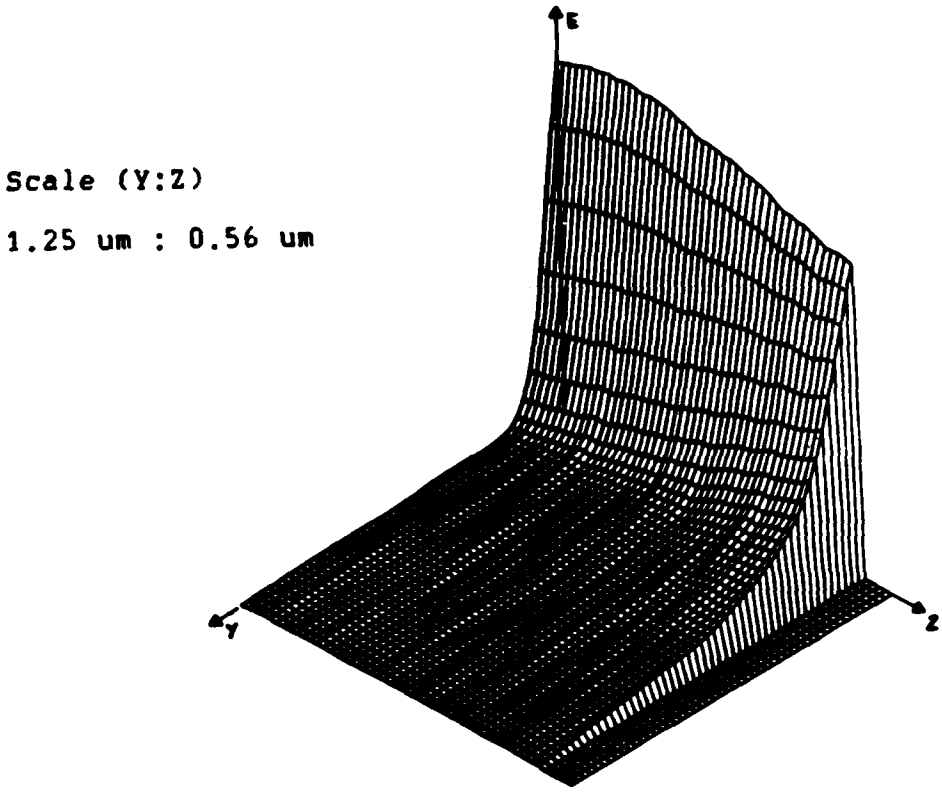

Figure 30. Energy deposition surface simulated with a 0.2 um beam of 10 keV electrons incident upon 0.5 um of PMMA on Silicon.

DOCUMENT CONTROL SHEET

Overall security classification of sheet UNCLASSIFIED

(As far as possible this sheet should contain only unclassified information. If it is necessary to enter classified information, the box concerned must be marked to indicate the classification eg (R) (C) or (S))

1. DRIC Reference (if known)	2. Originator's Reference	3. Agency Reference	4. Report Security Classification
	Memorandum 3690		U/C

5. Originator's Code (if known)	6. Originator (Corporate Author) Name and Location
	Royal Signals and Radar Establishment

5a. Sponsoring Agency's Code (if known)	6a. Sponsoring Agency (Contract Authority) Name and Location

7. Title

EXPOSURE MODELLING OF PARTICLE BEAM LITHOGRAPHY

7a. Title in Foreign Language (in the case of translations)

7b. Presented at (for conference papers) Title, place and date of conference

8. Author 1 Surname, initials	9(a) Author 2	9(b) Authors 3,4...	10. Date	pp. ref.
Broughton C	Mifsud V J			

11. Contract Number	12. Period	13. Project	14. Other Reference

15. Distribution statement

Unlimited

Descriptors (or keywords)

continue on separate piece of paper

Abstract

See Attached Sheet

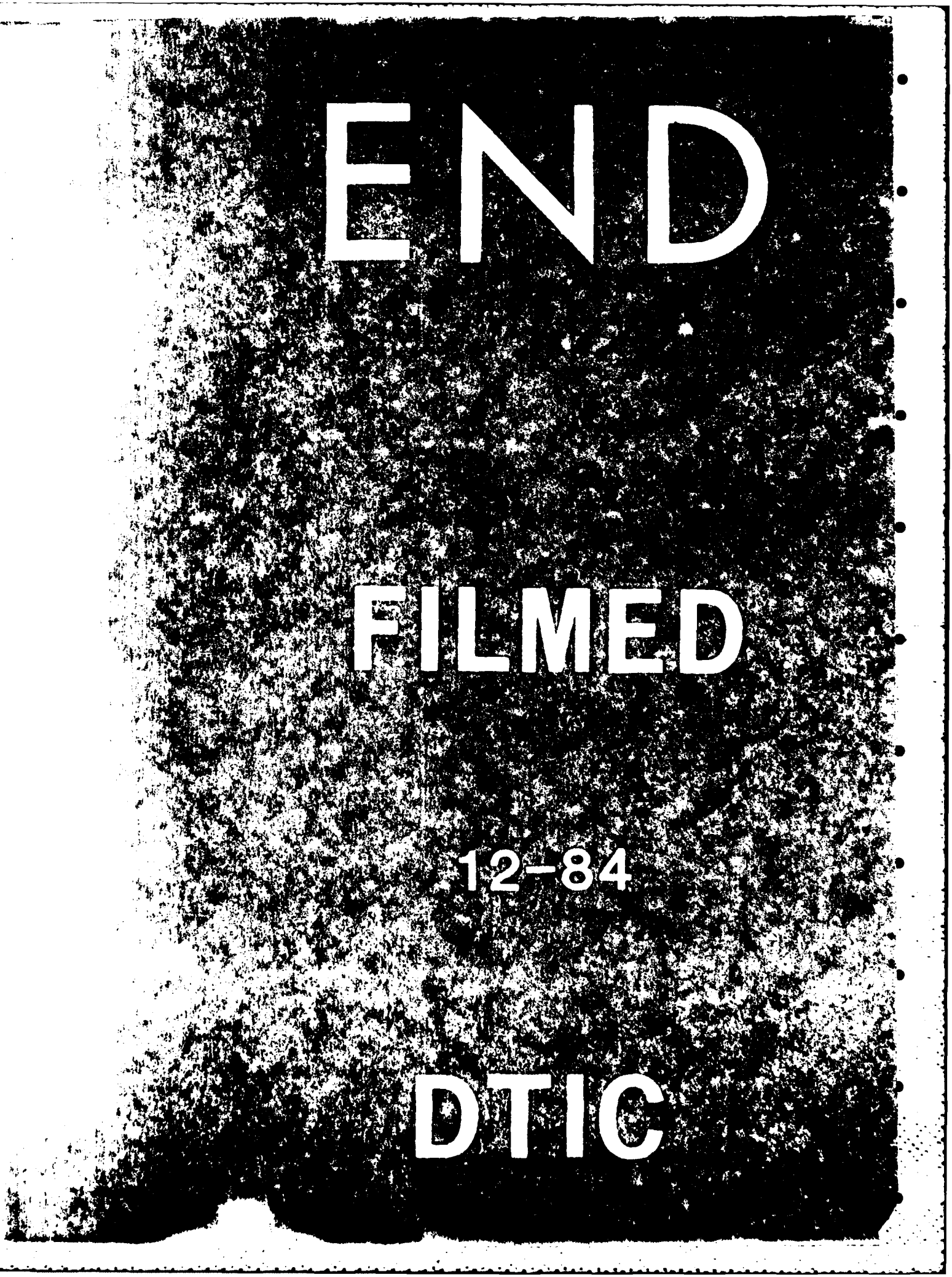
END
FILMED
12-84
DTIC